Quaternary Science Reviews 300 (2023) 107914

Contents lists available at ScienceDirect

Quaternary Science Reviews

journal homepage: www.elsevier.com/locate/quascirev

Invited review

Authigenic uranium deposition in the glacial North Atlantic: Implications for changes in oxygenation, carbon storage, and deep water-mass geometry

Y. Zhou [a, b, 1, *], J.F. McManus [a, b]

[a] Lamont-Doherty Earth Observatory of Columbia University, Palisades, NY, 10964, USA
[b] Dept. of Earth and Environmental Sciences, Columbia University, New York, NY, 10027, USA

ARTICLE INFO

Article history:
Received 7 February 2022
Received in revised form
4 December 2022
Accepted 5 December 2022
Available online 17 December 2022

Handling Editor: A. Voelker

Keywords:
Bottom water oxygen
Authigenic uranium
North Atlantic
Last glacial maximum

ABSTRACT

Oxygen in the ocean has essential ecological and climatic functions, and can be an important indicator of deep-ocean ventilation and carbon storage. Previous studies are divided on whether the subsurface North Atlantic, which today is well-oxygenated, had higher or lower oxygen levels during the Last Glacial Maximum (LGM). Crucially, the limited number of previous reconstructions precludes any conclusions regarding basin-wide patterns in past changes in oxygenation. Authigenic uranium in deep-sea sediments is a sensitive redox tracer that can shed light on bottom water oxygen. Here, we leverage published and new U- and Th-series isotope measurements from North Atlantic sediments to calculate the mass accumulation rate of authigenic uranium (aU MAR) during the Holocene and the LGM. We find that greater aU burial, reflecting lower-than-Holocene oxygen levels and correspondingly greater respired carbon storage, were persistent features of the LGM in the deep North Atlantic. The eastern basin was substantially less well-oxygenated than the western basin. This zonal contrast is possibly related to the farther advance and greater infilling to the east of the mid-Atlantic Ridge of deep waters originating from the Southern Ocean. An alternative explanation is the different residence time in the two basins of deep waters originating from the subpolar North Atlantic. Previous compilations of two nutrient tracers, $\delta^{13}C$ and Cd_W, are consistent with the varying-deep-circulation interpretation of our aU MAR dataset. The observed threshold behavior of aU or the pattern of export productivity, especially at high latitudes, may also have enhanced this west-east difference.

1. Introduction

Dissolved oxygen in the ocean is ecologically and climatically important. Because of the stoichiometric relation between oxygen and carbon during photosynthesis and respiration, oxygen utilization is a first-order indicator of the strength of the biological carbon pump (Volk and Hoffert, 1985). Additionally, oxygen is critical for marine life (Diaz and Rosenberg, 1995, 2008), including the maintenance of pelagic marine-life habitat (Stramma et al., 2012) and benthic organism diversity (Vaquer-Sunyer and Duarte, 2008). Oxygen concentrations at depth are also influenced by, and therefore indicative of, deep-ocean ventilation and abyssal circulation. Through the Atlantic meridional overturning circulation (AMOC), the modern deep North Atlantic is the best ventilated and oxygenated ocean basin (Garcia et al., 2018). Understanding how oxygenation evolved in the subsurface North Atlantic during different climate states is valuable for assessments of past ocean ecosystem health and carbon storage, and may provide insights for future projections.

To reconstruct the history of its oxygenation beyond the temporal range of modern hydrographic measurements, researchers have developed a range of geochemical and micropaleontological tools. Redox sensitive metals such as Mo (Arnold et al., 2004), V (Yarincik et al., 2000), Zu, Cu, Cd, Re (Janssen et al., 2014), Mn, Ni, Fe (Morford and Emerson, 1999), $\delta^{98}Mo$ (Riedinger et al., 2021; Siebert

Abbreviations: aU MAR, authigenic uranium mass accumulation rate; LGM, Last Glacial Maximum; NADW, North Atlantic Deep Water; AABW, Antarctic Bottom Water.

* Corresponding author. Lamont-Doherty Earth Observatory of Columbia University, Palisades, NY, 10964, USA
E-mail address: yuxin_zhou@ucsb.edu (Y. Zhou).
[1] Present address: Department of Earth Science, University of California, Santa Barbara, CA, 93106.

https://doi.org/10.1016/j.quascirev.2022.107914
0277-3791/

et al., 2003), and authigenic uranium (Klinkhammer and Palmer, 1991) have been utilized as bottom water oxygen proxies. Researchers have also taken advantage of the biological response to oxygen changes as proxies, including $\Delta\delta^{13}C$ (Hoogakker et al., 2015; Jacobel et al., 2020; McCorkle et al., 1990; McCorkle and Emerson, 1988; Thomas et al., 2022), $\delta^{15}N$ (Jaccard and Galbraith, 2012), alkenone concentration (Anderson et al., 2019), and benthic foraminifera assemblage (Baas, 1998; Schönfeld et al., 2003). Proxies from which oxygen may be determined indirectly as a result of its relationship with carbon include foraminifera shell weight (Barker and Elderfield, 2002; Broecker and Clark, 2001), benthic foraminiferal B/Ca (Rae et al., 2011), and benthic foraminiferal $\delta^{11}B$ (Foster and Rae, 2016).

Despite the diverse range of proxies available and more than two decades of research, reconstructions of the LGM North Atlantic bottom water oxygen are still limited (Fig. 1). A review of existing data shows gaps in the mid-latitude and subpolar western North Atlantic as well as the tropical eastern North Atlantic. This lack of reconstructions makes it difficult to extrapolate any detected oxygenation change during the LGM to the entire basin. Obtaining oxygenation data covering a broad spatial range may thus provide valuable new information about the pattern of oxygenation change during the LGM.

U- and Th-series isotope measurements are increasingly common in paleoceanographic studies, used to reconstruct dust flux, opal flux, ice-rafted debris (IRD) flux, and Pa/Th, among other paleoceanographic applications. An application that is sometimes overshadowed by these proxies is the potential of using the isotope measurements to derive authigenic uranium, a redox-sensitive proxy reflecting the deep-water oxygenation. Here, we leverage published and new U- and Th-series isotope measurements in the North Atlantic to calculate the mass accumulation rate of authigenic uranium (aU MAR). We make comparisons between the eastern and western basins, which are separated at depth by the mid-Atlantic Ridge (MAR), and also between the late Holocene (0–6 ka) and the LGM (19–23 ka) intervals. The multiple factors that can lead to aU changes are explored, and the compiled aU dataset is compared with published datasets of the widely utilized water-mass tracers $\delta^{13}C$ and Cd_W. To assess the proxy's uncertainty, we rate each core's quality based on seven criteria and calculate error propagation if not directly reported. Our study provides insight into glacial changes in the deep North Atlantic, and demonstrates the value of compiled aU MAR as a qualitative indicator of oxygen.

2. Materials and methods

2.1. U systematics

Uranium can serve as a bottom-water oxygen proxy because dissolved uranium is redox-sensitive, being highly soluble in the presence of oxygen and observed to diffuse from bottom water into suboxic and anoxic sediments and precipitate as solid uraninite (Klinkhammer and Palmer, 1991; Thomson et al., 1990). This precipitated uranium is termed “authigenic” to differentiate it from the lattice-bound uranium from detrital sources. Bottom-water oxygen is regulated by a balance between ventilation by deep circulation and the respiration of organic carbon exported to depth from the near-surface ocean. The former supplies oxygen, while the latter consumes it. Therefore, aU is an indicator of the net oxygen balance. To use aU as a proxy for either ventilation or organic carbon export alone, the other competing process must either be constrained by observations or assumed to be approximately constant.

In practice, aU in sediments is the portion of non-detrital uranium within the total pool of uranium measured in an individual

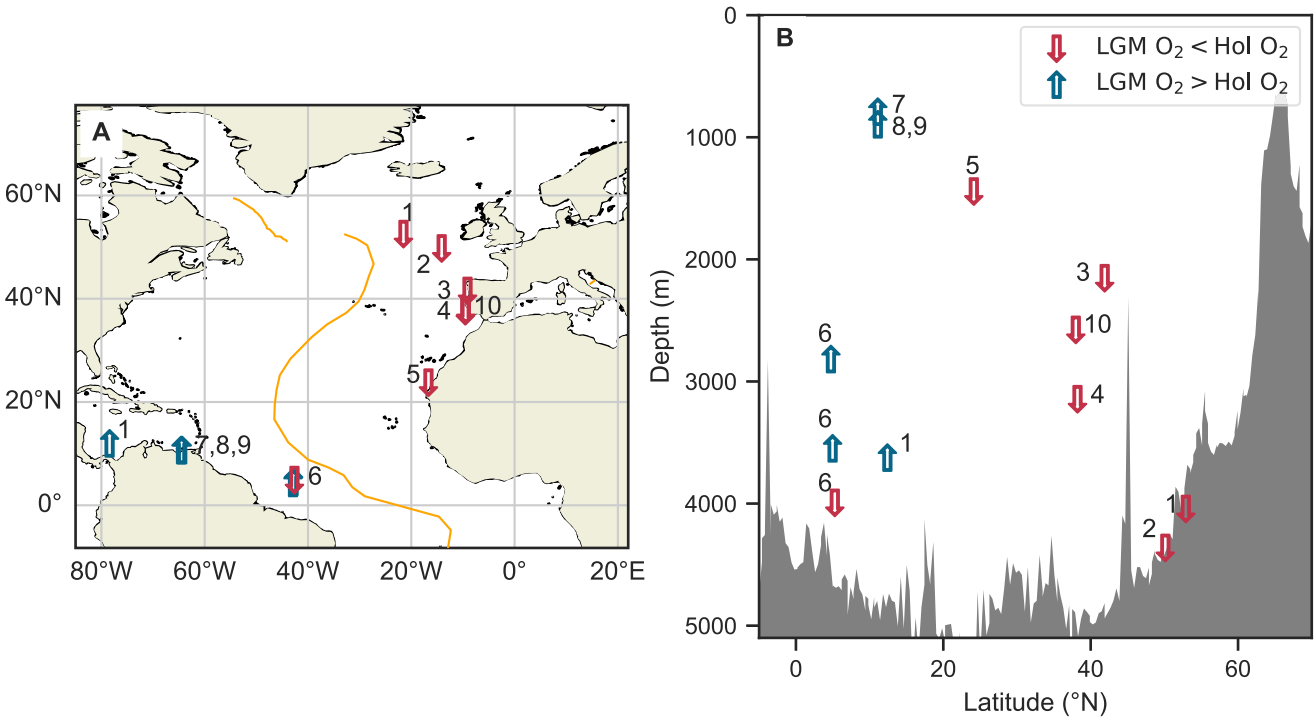

Fig. 1. Existing reconstructed bottom-water oxygen comparisons between the LGM and the Holocene, in map view (**A**) and transect view (**B**). 1: (Yu et al., 2010). 2: Thomson et al. (1990). 3: Baas (1998). 4: Hoogakker et al. (2015). 5: (Martinez et al., 2000). 6: Broecker and Clark (2001). 7: (Dean, 2007). 8: (Haug et al., 1998). 9: Yarincik et al. (2000). 10: Thomas et al. (2022).

sample. Detrital uranium in deep-sea sediments can be estimated by assuming a constant ratio with common thorium (^{232}Th) within a limited range (~0.4–0.7) observed in modern ocean basins (Henderson and Anderson, 2003). In this study we use a ratio of 0.6 for detrital ^{238}U/^{232}Th, based on the similar range determined in previous downcore studies (Henderson and Anderson, 2003; McManus et al., 2004, 1998; Missiaen et al., 2018; Zhou et al., 2021). The calculation of aU is thus:

$$aU = U - 0.6 \times Th$$

2.2. aU MAR

Holding the diffusive flux of uranium constant, a lower sediment accumulation rate would lead to more aU accumulation for a given amount of sediment. Therefore, while the concentration of aU provides useful information, the mass accumulation rate of aU (aU MAR) additionally accounts for the depositional rate of sediments. The aU MAR is derived as follows:

$$aU\ MAR = MAR \times aU$$

Note that $^{230}Th_{xs}$-based mass flux may not be valid for tracers supplied by diffusion because it only accounts for the vertical particle rain rate and not syndepositional sediment redistribution. Therefore, the MAR may be more suitable for inferring the sediment redox state and thus calculating the diffusive flux of uranium into deep-sea sediments.

MAR is calculated as:

$$MAR = LSR \times DBD$$

Where LSR is the linear sedimentation rate, and DBD is the dry bulk density. LSR can be approximated by assuming a constant sedimentation rate between age model tie-points. DBD is measured in some deep-sea cores, especially those collected via the Ocean Drilling Program/International Ocean Discovery Program. Some cores do not have DBD data available but have wet bulk density (WBD) and porosity (POR) data. DBD can be calculated as:

$$DBD = WDB - POR \times \varrho_{sw}$$

Where ϱ_{sw} is the seawater density.

2.3. Dataset description

We compiled all published studies in the study region that report bulk sedimentary U and Th data. The studies must have data during the late Holocene (0–6 ka) or the LGM (19–23 ka), the two intervals over which we average the data, regardless of the data resolution. The definition of the two intervals follow previous conventions (Mix et al., 2001; Schmittner et al., 2017), and we tested the robustness of our definition to ensure that alternative interval definitions do not produce contradictory results (Figs. S1–2). The cores included in the dataset are limited to the North Atlantic, between −5°N and 70°N. In 49% of the cores, the only data available are coretop measurements, while the rest of the compiled study cores include downcore data. In all, there are 3840 data points from 185 cores drawn from 45 studies (Data S1). Data reporting practices vary among these studies. Of the 185 cores compiled, 75 cores only have radionuclide concentration data reported instead of activity and, for the sake of uniformity, these were all converted using their respective decay constants (Cheng et al., 2013). Five of the cores have reported activity ratios and the activity of one of the isotopes. In these cases, the activity of the second isotope was deduced, and error propagation was back-calculated. In one case (Frank and Eisenhauer, 1996), the ^{234}U/^{238}U error was smaller than ^{234}U error, and back-calculating ^{238}U error was impossible. In this case, it was assumed that ^{234}U/^{238}U and ^{234}U were measured and ^{238}U was calculated. Some studies do not report whether the error was 1σ or 2σ, in which case we assume it is 2σ.

About one-third of the cores in this dataset have dry-bulk density (DBD) data that allow the direct calculation of MAR. The average of the available DBD data points is 0.92 g/cm^3 (σ = 0.29 g/cm^3), which we use as a first-order estimate for cores without DBD measurements.

We supplement the aU compilation with new measurements from three cores. DY081-GVY005 (58° 36.6′N, 43° 46.8′W, water depth 1907 m) is located south of Greenland, collected during the ICY-LAB cruise (Hendry et al., 2019). To establish age control, we measured ^{14}C at five depths on 300–400 planktic foraminifera *Neogloboquadrina pachyderma* at the NOSAMS-WHOI facility and calibrated it with Marine13 (Reimer et al., 2013) (Data S2; Fig. S3). EW9303-GGC31 (50° 34.2′N, 46° 21′W, water depth 1796 m) was retrieved from Orphan Knoll. We update the published age model of this core (Bond and Lotti, 1995) with Marine13 calibration. IODP U1313 (41° 00′N, 32° 34.4′W, water depth 3413 m) is from the western flank of the mid-Atlantic Ridge and is a reoccupation site of DSDP 607. We used a published age model based on X-ray diffraction data and the identification of Heinrich events (Naafs et al., 2013). While this core has some published U-series data (Lippold et al., 2016), we increased the temporal resolution by three-fold. Bulk sediment samples of about 100 mg were spiked, digested, and purified to prepare for U and Th isotope activity measurement (Fleisher and Anderson, 1991). The analysis was done on an Element Plus inductively coupled plasma mass spectrometer (ICP-MS) at Lamont-Doherty Earth Observatory (results discussed in Supplementary Text S1).

We deploy a quality-rating scheme to assess each core's data (Table S1). Seven criteria are used for evaluation, including considerations for the reporting practices, age model quality, and instrument quality. Regarding reporting practices, we tallied the percentages of data points that come with raw isotopic activities, those with error estimates on isotopic activities, and those that have dry bulk density measurements. In terms of age models, we counted the percentages of data points with radiocarbon-based age models, those with radiocarbon measurements calibrated with the Marine13 curve (Reimer et al., 2013), and those with benthic-δ^{18}O-based age models. Lastly, we calculated the percentage of data points that were measured with mass spectrometry instead of alpha counting, which is less accurate (Li et al., 1989).

2.4. Chronology

One challenge for any data-compilation project is to ensure the chronologies of different cores are consistently documented. Radiocarbon (^{14}C) dating is a commonly applied chronological approach among sedimentary studies within our study intervals. However, the calibration curve of measured ^{14}C to calendar age has been updated over time, rendering such chronologies moving targets. Here, whenever raw ^{14}C ages were reported in the literature, Marine13 is used to convert them to calendar ages (Reimer et al., 2013) using a standard 400-year marine reservoir correction. Some studies do not say whether the published radiocarbon-based ages are calibrated or not, and some datasets come from online repositories without accompanying documentation to explain the age model procedure. In these cases, we choose from two options. If the study was published before 1990, the year Bard et al. (1990) became available, the ^{14}C age was probably not calibrated, and

we calibrate the age using Marine13. If published after 1990, some calibration was likely performed, and we present the age as is, given the difficulty of back-calculating the raw ^{14}C age without knowing the specific calibration used.

Some papers cited other studies for their chronology. The original study that published the chronology can be found in Supplementary Data S1. In one case (Mangini, 1978), the chronology of the original paper was later updated by a newer study, which is why the age model column cites a paper published later than the original citation (Data S4).

3. Results

3.1. Comparison of the last-1-kyr aU MAR and hydrographic bottom water oxygen

Coretop and recent sediments throughout the North Atlantic display generally low aU MAR, with some spatial structure. We compared our last-1-kyr aU MAR dataset to the bottom water oxygen concentration ($[O_2]_{bottom}$) data from the World Ocean Atlas 2018 (WOA18 (Garcia et al., 2018); Fig. 2). The result of this comparison is not overly sensitive to the interval that we use to define the coretop (Figs. S4 and 5). High aU MAR data points coincide with low $[O_2]_{bottom}$ along the coasts of Northwest Africa and Southeastern US (Fig. 2A and B). The scatter plots juxtaposing the oxygen concentration with aU concentration and aU MAR show an approximately inversely linear relationship (Fig. 2C and D). The scatter plots also reveal that $[O_2]_{bottom}$ may have to decline below a threshold value (~220 μmol/kg) in order to induce aU precipitation. Therefore, the WOA18 bottom water oxygen and aU dataset have some first-order agreement. Both capture the low-oxygen environment in the subtropical and tropical coastal regions, which could be related to the high export productivity of wind-driven upwelling and the accompanying intensified decomposition of organic materials that consumes oxygen at depth. The aU dataset missed the low $[O_2]_{bottom}$ of Baffin Bay (Fig. 2A and B), but only one

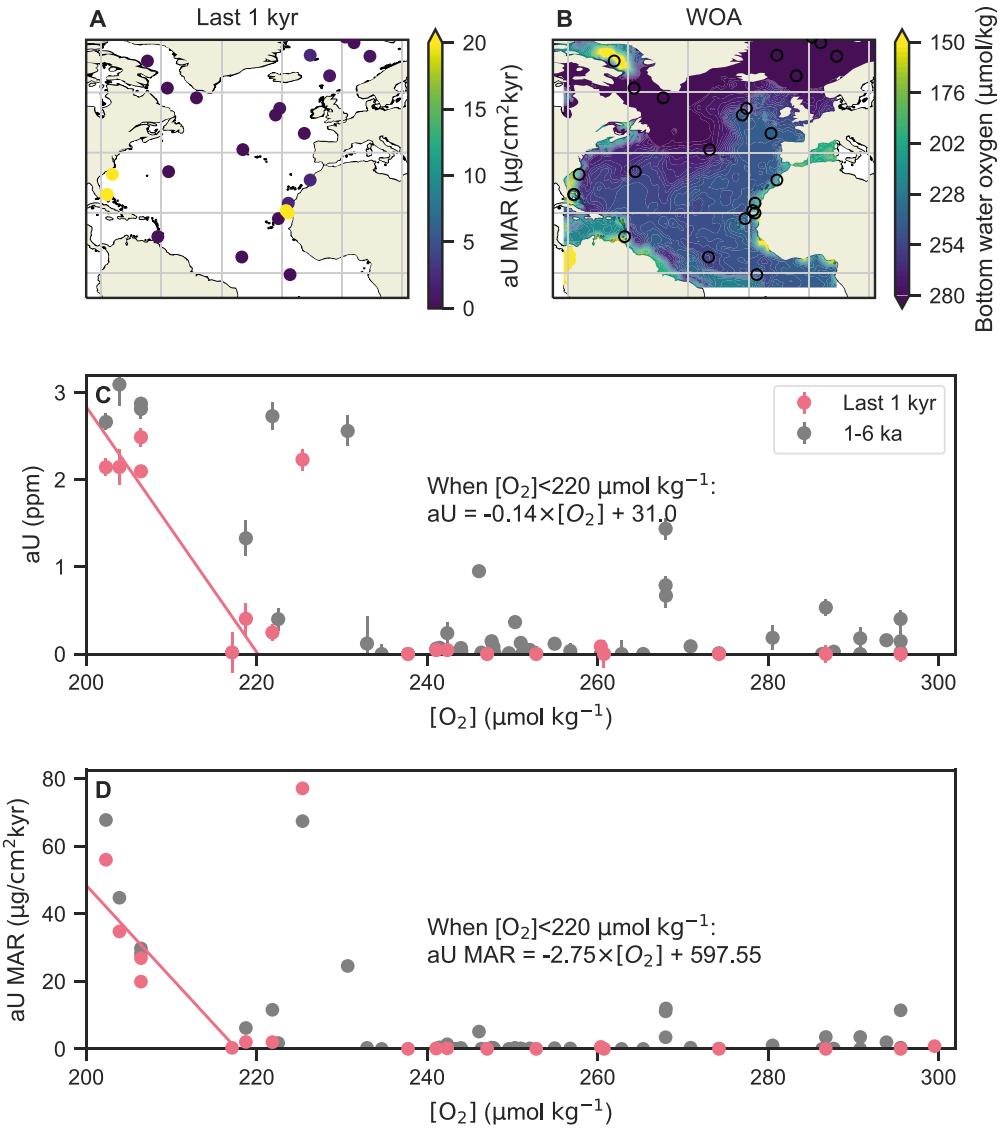

Fig. 2. Comparison of aU MAR dated to the last 1 kyr from our dataset and hydrographic measurement of the bottom water oxygen saturation. (A) Average aU MAR of the last 1 kyr. (B) World Ocean Atlas 2018 (WOA18) oxygen concentration at the deepest depth available (Garcia et al., 2018). (C and D) Scatter plots illustrating the relation between last 1 kyr and 1–6 ka aU concentration (C) and aU MAR (D) from our dataset and WOA18 oxygen concentration at the deepest depth available. In (B) Circles mark the locations of core sites in (A). In (C) and (D), the regression lines as well as their equations are presented. For the regression, only sites with data during the last 1 kyr and where oxygen concentrations are less than 220 μmol/kg are included.

data point from our dataset exists in the region and it is located just outside of the zone of low-oxygen bottom water. One data point in the scatter plots (Fig. 2C and D), measured in a core retrieved from the coast of Northwest Africa (Adkins et al., 2006), appears to be an outlier of the inverse linear trend between $[O_2]_{bottom}$ and aU. The number of observations from which the WOA18 is constructed is low in the Northwest coast of Africa in general (Garcia et al., 2018). Only three observations are available in the grid cell (1° by 1°) that the core is in. The low number of observations, together with the relatively steep local bathymetry gradient, can lead to greater uncertainty of the bottom water oxygen at this site and could be the reason this data point is an outlier.

3.2. aU MAR dataset Holocene and LGM comparison

The patterns of aU MAR in the North Atlantic reveal substantial differences between the Holocene and the LGM (Fig. 3).

During the Holocene (Fig. 3A), high aU MAR (>15 μg/cm^{2}kyr) are mostly seen in coastal regions of the mid-latitudes (15–35°N), including the coast of Northwest Africa and the Southeastern US. Sporadic intermediate aU MAR (5–15 μg/cm^{2}kyr) can be found in the Hatton-Rockall Basin, east of Newfoundland, and the Barbados Basin. The clustering of relatively high aU MAR in coastal regions is also apparent in the transect view (Fig. 3D), as the shallower sites generally show higher aU MAR.

During the LGM (Fig. 3B), sites of high aU MAR (>15 μg/cm^{2}kyr) extended further into the interior North Atlantic and can be additionally found in the Bermuda Rise, the Iberian Margin, and the Central Equatorial Atlantic. Intermediate aU MAR (5–15 μg/cm^{2}kyr) can be found in the slopes of the mid-Atlantic Ridge. Amid a general trend of higher aU MAR during the LGM than the Holocene, however, some sites with high Holocene aU MAR had lower values during the LGM. These include sites on the east coasts of Florida and Barbados, as well as the southern Baffin Bay. The scattered expansion of the high aU MAR into greater depths can be seen in the transect view (Fig. 3E). The reverse of that trend – lower aU MAR

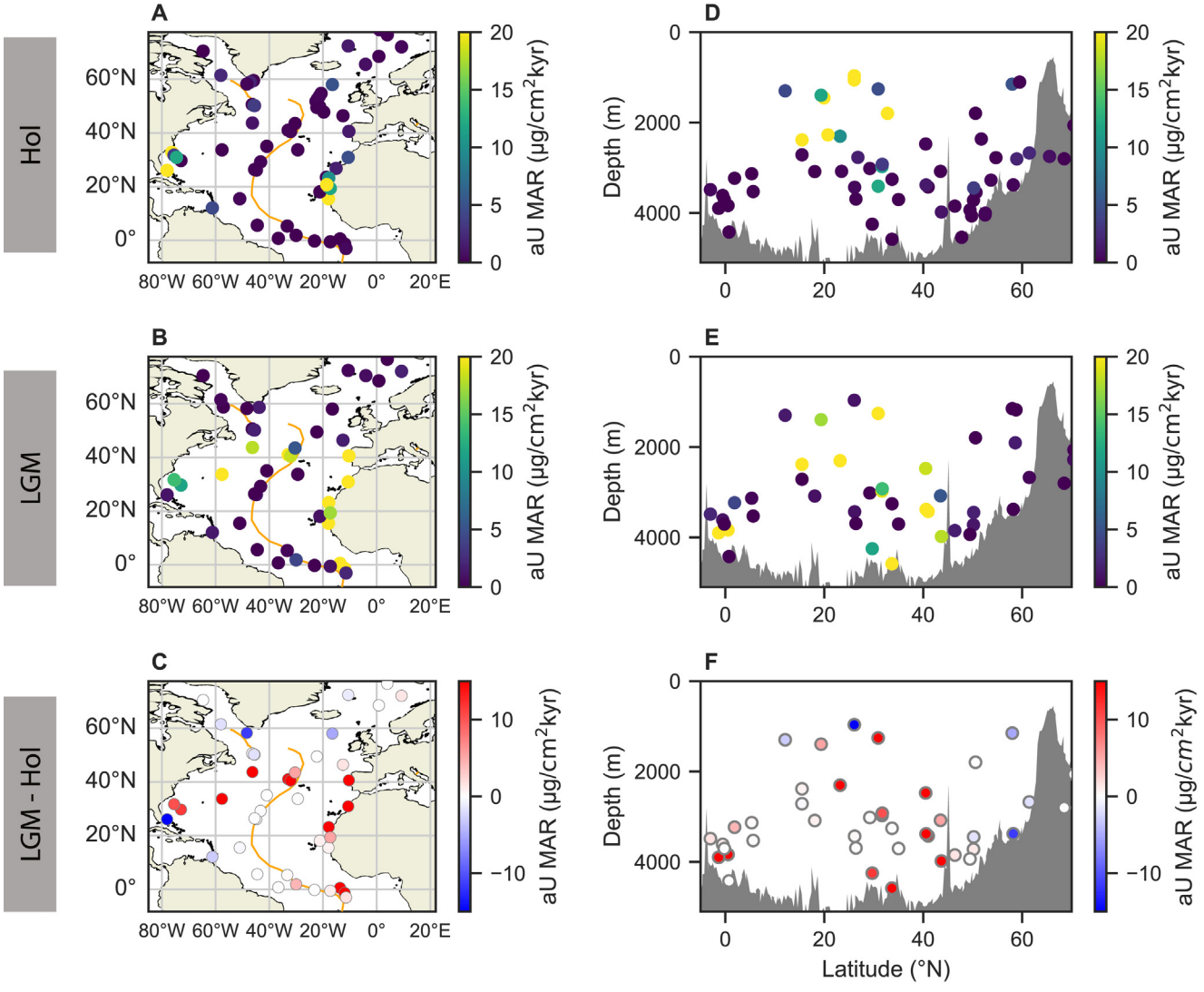

Fig. 3. The aU MAR dataset in map (A, B, C) and transect (E, F, G) views during the late Holocene (0–6 ka; A, D), the LGM (19-23ka; B, E), and difference between the two periods (LGM - late Holocene; C, F). The orange lines in (A–C) are the mid-Atlantic Ridge.

during the LGM – can be seen in sites that occupy intermediate water depths.

The comparison between the two periods in the map view (Fig. 3C) shows positive values (higher aU MAR during the LGM) along the mid-Atlantic Ridge, the mid-latitude North American coast, and the coasts of Europe and Africa. Negative values (higher aU MAR during the Holocene) are mostly limited spatially to the high- and low-latitude coastal regions. In the transect view (Fig. 3F), the division between positive and negative aU MAR (LGM-Holocene) occurs as shallow as 1000 m at 30°N. A line between the two contrasting responses occurs deeper at higher and lower latitudes.

3.3. Comparison of the east/west transect

We examined the dataset east and west of the mid-Atlantic Ridge separately (Fig. 4). Relatively high LGM aU MAR in the west basin is limited to mid-depth locations in the mid-latitudes and deep cores in the west transect (Fig. 4C). That limited range of higher LGM aU MAR is in contrast to the east transect, where the relatively high LGM aU MAR is more expansive meridionally (0–45°N) and vertically (1000–4000 m) than in the west (Fig. 4F).

3.4. Uncertainty analysis

The lack of uncertainty constraints on the age model and DBD in our dataset makes it difficult to analyze the uncertainty of MAR. Hence, we do not attempt to calculate the aU MAR uncertainty. We instead analyze the uncertainty associated with the aU concentration reconstructions.

During the Holocene, the 2σ uncertainty of aU ranges from 0.019 ppm to 0.36 ppm, with a median of 0.14 ppm (Figs. S6A and D). During the LGM, the 2σ uncertainty of aU is somewhat higher, which is expected given the higher aU of this period. The LGM aU 2σ uncertainty ranges from 0.04 ppm to 1.76 ppm, with a median of 0.19 ppm (Figs. S6B and E). The difference between the Holocene and LGM aU has 2σ uncertainty that ranges from 0.04 ppm to 0.5 ppm, with a median of 0.23 ppm. The lowest 2σ uncertainty seems to be along the mid-Atlantic Ridge. Several cores, OC437-07_GC49, PS1533-3, and GIK12310-4 (Data S1), have high

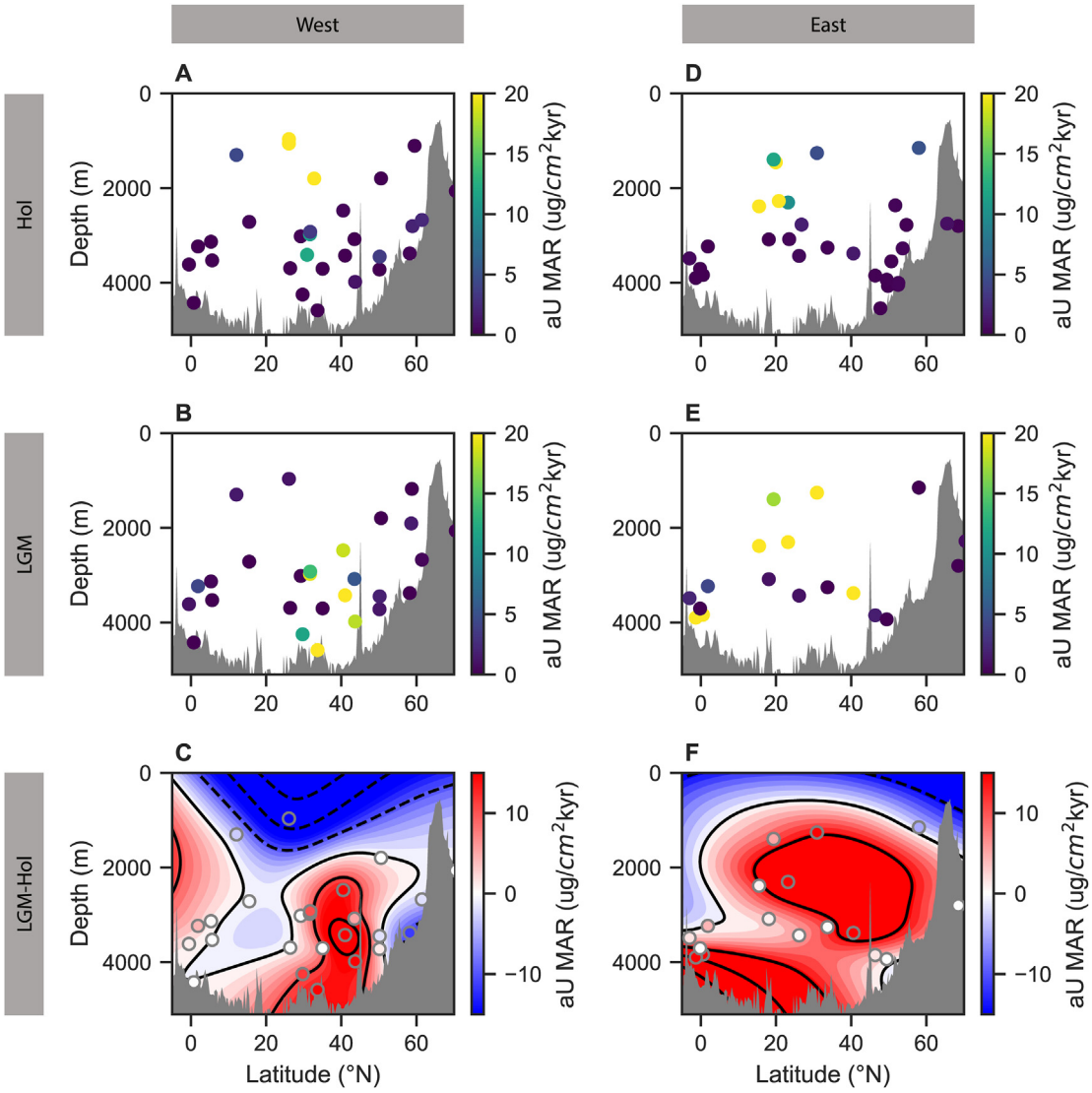

Fig. 4. Comparison of the eastern (**A, B, C**) and western (**D, E, F**) North Atlantic transects of aU MAR during the Holocene (**A, D**), the LGM (**B, E**), and the difference between the two periods (LGM-Holocene; **C, F**). The west-east division is along the mid-Atlantic Ridge.

uncertainty. One core, GIK12310-4 (Mangini, 1978), stands out for its high uncertainty, which may be the result of it being the oldest study included in this dataset and likely generated by alpha-counting rather than the now-common approach of mass spectrometry.

3.5. Data quality rating

An overview is compiled for the quality rating scheme (Table S1), and the transects filtered by the quality score are presented (Fig. S7). Based on the screening of the quality rating, the aU transect patterns mostly stay the same if only cores with score ≥ 4 are included, and the west-east difference ceases to exist if the score threshold is raised to 5. The map view of the quality score screening does not show regional bias between cores that have most of the information needed for the aU MAR calculation and those that needed additional assumptions and thus came with added uncertainty (Fig. S8). The overall spatial pattern remains similar unless the score threshold is raised to 6.

4. Discussion

4.1. Factors influencing aU precipitation

Two trends stand out in our observations. One is the generally higher aU MAR during the LGM than the Holocene in subsurface waters (Fig. 3C, F). The other is that these higher-than-Holocene aU MAR values during the LGM are more expansive in the eastern basin (Fig. 4C, F). Before discussing the implications of the two trends, we first consider the mechanism of uranium precipitation and potential challenges to the straightforward interpretation of aU MAR data as a redox-sensitive proxy indicative of past changes in oxygenation.

Most of the uranium in the ocean forms highly soluble carbonate complexes (Langmuir, 1978). These uranium complexes behave mostly conservatively and have a residence time of 300–600 kyrs (Dunk et al., 2002; Ku et al., 1977; McManus et al., 2005; Morford and Emerson, 1999). A small portion of the oceanic uranium, when encountering reducing environments, forms solid uraninite (UO_2) and precipitates in sediments (Anderson, 1982; Morford and Emerson, 1999). Instead of the reduction step occurring above the water-sediment interface, uranium diffuses from bottom water into suboxic and anoxic sediments and precipitates or is adsorbed onto sediment solids (Barnes and Cochran, 1990; Cochran et al., 1986; Zheng et al., 2002). The reduction of uranium seems to occur only when a redox potential threshold is reached (Algeo and Li, 2020; Algeo and Liu, 2020; Bennett and Canfield, 2020; Lu et al., 2022). In our dataset, when considering only data points measured on sediments younger than 1 kyr, this threshold behavior is clearly evident (Fig. 2C and D). Both aU concentration and aU MAR are negligible at high oxygen concentrations and begin to increase as $[O_2]$ decreases below 220 μmol/kg. As uranium precipitates at some depth in the sediment column, a sub-seafloor concentration gradient forms in the porewater that further drives the downward diffusive flux of dissolved uranium from the overlying seawater. Sedimentary aU peaks form as a result. Studies have proposed different hypotheses on the exact mechanism of uranium reduction that leads to sedimentary precipitation. Uranium reduction has been observed to coincide with iron reduction (Cochran et al., 1986) or sulfate reduction (Klinkhammer and Palmer, 1991) in anoxic sediments. It has also been proposed that uranium reduction is controlled by iron- and sulfate-reducing and often anaerobic bacteria (Francis et al., 1994; Lovley et al., 1993, 1991; Lovley and Phillips, 1992; Sani et al., 2004; Senko et al., 2002; Tucker et al., 1996).

Despite the lack of consensus on the details of this process, the clear redox-sensitive nature of uranium precipitation can still provide a valuable perspective on the history of the redox potential changes. However, aU MAR cannot serve as a redox proxy universally without due considerations of the specific depositional environment. Age offsets, accumulation rate changes, and “burndown” effects can all influence the aU MAR observation. In each case we find the potential influences relatively small or unlikely, allowing a deep-circulation interpretation to be made with some confidence.

In nearly all cases, the deposition of authigenic uranium is believed to occur some centimeters beneath the sediment-water interface (Francois et al., 1993). The resulting offset between sediment age and the time of aU deposition therefore means that the apparent age of aU is somewhat older than the age of deposition (Jacobel et al., 2020). However, this offset is expected to be small in the North Atlantic because of the generally higher sediment accumulation rates (Costa et al., 2020). We estimate the age offset to be on the order of a few centuries and no more than two thousand years in a typical sediment environment in our study region (Supplementary Text S2). While this potential offset presents a challenge to assessing millennial variations in aU deposition, it has little influence on our assessment of the LGM and Holocene intervals.

Changes in sediment accumulation rate could influence the measured aU concentration. If the flux of precipitated uranium remains constant, a lower sediment accumulation rate would lead to more aU accumulation for a given amount of sediment (Francois et al., 1993). In the North Atlantic, sediment accumulated faster during the glacial interval than in the Holocene, primarily because of enhanced detrital deposition from surrounding continents, including by ice-rafting (Costa et al., 2020; McManus et al., 1998). The sedimentation influence is opposite to the observed change in aU, and therefore higher aU MAR during the LGM exists despite Glacial-Holocene changes in the sediment accumulation rates, confirming that the change reflects greater aU burial.

Precipitated uranium can become soluble and remobilized upon the subsequent diffusion of oxygenated water into sediment porewater. Either the so-called “burndown” effect (Colley et al., 1989; Colley and Thomson, 1985; Jacobel et al., 2020; Shaw et al., 1994; Thomson et al., 1990) or bioturbation (Zheng et al., 2002) could remove the sedimentary signal through the subsequent oxidization and return to solution of previously accumulated aU. These effects mean that low aU cannot provide a quantitative measure of high seawater oxygen concentrations in the past. The rapid burial of sediments creates a barrier that more readily isolates aU and makes the combined effects of burndown and bioturbation less influential. It has been estimated that sediments accumulating at less than 2 cm/kyr may be particularly susceptible to the effect of burndown (Mangini et al., 2001). In comparison, the median of the sedimentation rates of the cores in our dataset is 5.9 cm/kyr. As a result, the relatively high sediment accumulation rates in the North Atlantic are advantageous for preserving and documenting the signal of aU deposition. Nevertheless, we recognize that any observed absence of aU does not preclude its previous existence. The preserved aU signal in these sediments is likely to reflect the original redox conditions, while serving as a minimum estimate of aU deposition and implied deoxygenation. The “burndown” effect and bioturbation make it all the more important to look at broad patterns of aU changes. Our compilation thus minimizes the risk of erroneous interpretations based on a more limited data coverage.

We assess the potential existence of the burndown effect and bioturbation in five cores (Fig. 5). If burndown and bioturbation indeed played important roles in determining the aU concentration in these cores, we expect that the cores with relatively high sedimentation rates to have unaltered aU peaks. Two cores, IODP

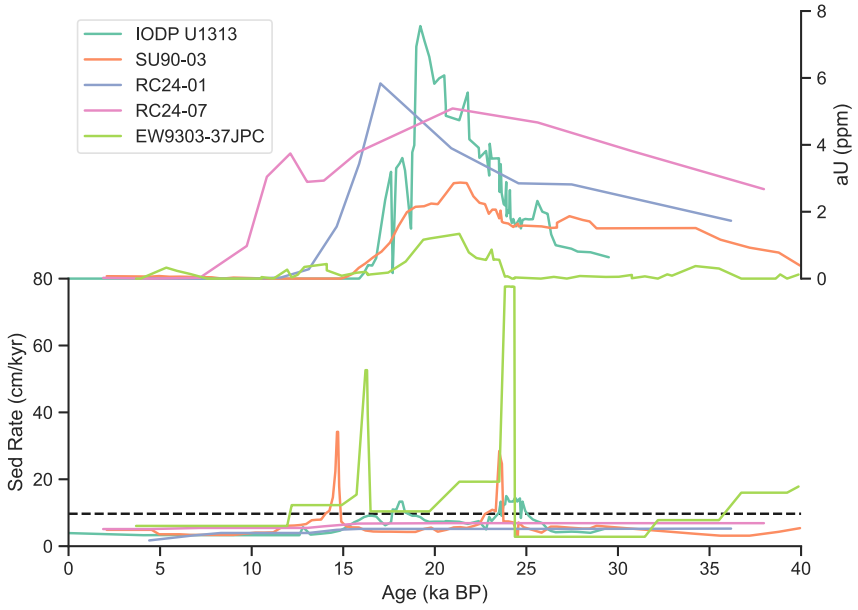

Fig. 5. Case study of aU concentration and sedimentation rates of five cores. The dashed black line in the lower panel is the mean sedimentation rate of our dataset for the past 30 kyr.

U1313, SU90-03, were retrieved from sites in the mid-latitude central North Atlantic. Two other cores, RC24-01, and RC24-07, were retrieved from sites in the tropical eastern Atlantic. The shapes of the glacial peaks in aU range from narrow (IODP U1313) to broad (RC24-07). The fifth core, EW9303-37JPC, was retrieved from a site in the northwest Atlantic. While EW9303-37JPC has the highest sedimentation rate during the LGM and deglaciation, its aU concentration peak is the lowest among the cores. As discussed previously, a higher sedimentation accumulation rate could lead to less aU accumulation for a given amount of sediment (Francois et al., 1993). We could be seeing that effect here. On the other hand, while tropical core RC24-01 has the lowest overall sedimentation rate, it contains a high concentration of aU. Its asymmetrical peak shape (steeper drop-off upcore from the peak) may be the result of moderate burndown or bioturbation, but the aU concentration in this core remains the second highest of all five cores. Overall, the lack of a strong positive relationship between sedimentation rate and aU concentration in the five cores shows that the range of relatively high sedimentation rates in the North Atlantic helps mitigate the alteration effect of burndown and bioturbation, and thus preserves a sufficient proportion of the original signal to allow a robust interpretation.

4.2. Comparison with Cd_W and $\delta^{13}C$ datasets

While aU MAR can be used to track the consumption of oxygen through remineralization, another approach to reconstructing deep waters focuses on proxies of the nutrient products of that process. Cd_W and $\delta^{13}C$ are two examples of the latter approach, and serve as proxies for the nutrients (i.e. phosphate and nitrate) associated with the production and decomposition of organic matter. Because North Atlantic Deep Water (NADW) and Antarctic Bottom Water (AABW) have distinctly different nutrient concentrations, Cd_W and $\delta^{13}C$ have often been used as water mass tracers. Low Cd_W and high $\delta^{13}C$ are indicative of the presence of NADW, while the opposite suggests the increased influence of AABW. It is worth noting that these proxies are both also influenced by respiration at depth and are therefore not truly conservative tracers (Broecker and Maier-Reimer, 1992; Gebbie, 2014; Lynch-Stieglitz, 2003; Oppo and Horowitz, 2000). Moreover, unlike trace metals (e.g. Cd) that only circulate in the ocean, carbon (and therefore a portion of any $\delta^{13}C$ signal) is additionally exchanged between the air and sea (Lynch-Stieglitz et al., 1995; Oppo and Fairbanks, 1989). In the North Atlantic, the factors that control the air-sea isotopic equilibration mostly vary meridionally, and comparisons between the east and west basins are thus not expected to be influenced by air-sea exchange (Lynch-Stieglitz, 2003). We compare our aU MAR results with the compilations included in a $\delta^{13}C$ data-modeling comparison study (Hesse et al., 2011) that relied heavily on previous data reconstructions (e.g., Curry and Oppo, 2005), and in a separate Cd_W study (Marchitto and Broecker, 2006) (Figs. 6–8). Together, the three proxies provide a consistent picture of the bottom water nutrients during the LGM.

In map view, all three proxies are consistent with a large area of the central North Atlantic having higher nutrients in bottom waters during the LGM than the Holocene (Fig. 6C, F, I). Comparatively low nutrient levels can be found in the shallower coastal regions, including the Caribbean Sea and neighboring regions, south of Iceland, and east coasts of Florida and Barbados. The consistency of the three proxies is a reassuring sign that the aU MAR offers comparable information on high-nutrient water as the two conventional nutrient proxies.

In both the eastern and western transects, all three proxies display values consistent with higher LGM oxygenation levels at depths compared to the Holocene (Figs. 7 and 8 C, F, I). We infer that the bottom water oxygen-deprivation was more severe in the LGM than Holocene, and that the respired carbon inventory in the glacial North Atlantic must have been substantially higher, also consistent with complementary evidence from previous studies (Mangini et al., 2001; Yu et al., 2016). Our back-of-the-envelope calculation

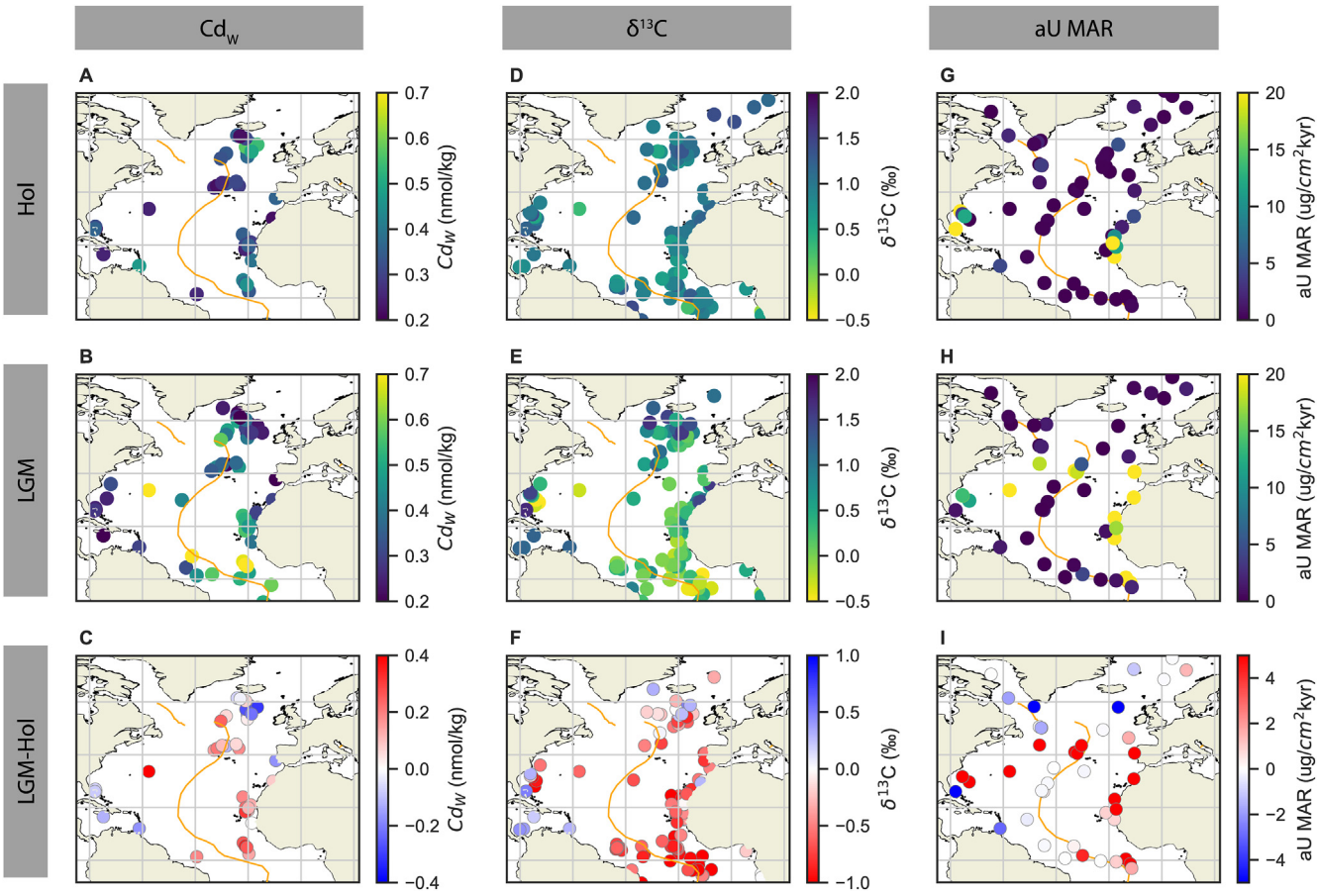

Fig. 6. Comparison of Cd_W (**A, B, C**) (Marchitto and Broecker, 2006), $\delta^{13}C$ (**D, E, F**) (Hesse et al., 2011), and aU MAR (**G, H, I**) (this study) in map view during the Holocene (**A, D, G**), the LGM (**B, E, H**), and the difference between the two periods (LGM-Holocene; **C, F, I**).

shows that the changes in the deep North Atlantic could have amounted to ~40 Gt of additional carbon storage (Supplementary Text S3) to that sequestered in the glacial Pacific and Southern oceans (Anderson et al., 2019; Gottschalk et al., 2016; Jaccard et al., 2016; Jacobel et al., 2020; Sarnthein et al., 2013). This independent evidence of respired carbon in the deep Atlantic is consistent with previous reconstructions from aU (Chase et al., 2001; Kumar et al., 1995), $[O_2]$ (Hoogakker et al., 2015), $[CO_3^{2-}]$ (Sosdian et al., 2018; Yu et al., 2016), and modeling (Menviel et al., 2017). Recent studies suggest that the respired carbon increase is primarily the result of the replacement of northern-sourced deep water by southern-sourced deep water, rather than changes in remineralization (Freeman et al., 2016; Oppo et al., 2018). Considering the relation between respiration and nutrient availability, our results also agree with the previous findings on nutrient deepening (Boyle, 1988; Bradtmiller et al., 2010). Lastly, our results are consistent with the suggestion of a very early study that was conducted without the benefit of geochemistry but nevertheless arrived at similar conclusions regarding glacial water mass geometry in the deep Atlantic (Streeter and Shackleton, 1979).

Notably, the boundaries between positive and negative LGM-Holocene differential values are shallower in the eastern transect for all three proxies. In the case of Cd_W, it was noted in the original publication that similar LGM Cd_W values are seen at a shallower depth in the eastern transect than the west (Marchitto and Broecker, 2006) (Figs. 7 and 8C). The west-east difference is also pronounced in $\delta^{13}C$, where the boundary between positive and negative LGM-Holocene differential values reached ~4000 m depth in the subtropical region of the western transect (Fig. 7F). In the eastern $\delta^{13}C$ transect, that same boundary barely appeared below 2000 m (Fig. 8F). While the $\delta^{13}C$ and Cd_W compilations both lack data in the high-latitude western transect, aU MAR fills in that gap and shows that glacial deep waters north of 50°N were mostly dominated by lower LGM values (lower nutrient and higher oxygen) than the Holocene.

The west-east difference of our dataset in oxygenation in deep waters separated by the mid-Atlantic Ridge (Fig. 4C, F) could be due to three factors — threshold behavior in aU precipitation, a zonal gradient in the supply of particulate organic carbon to the sediment (i.e., export production), and contrasting deep-water mass distributions. Below we consider the three scenarios and discuss their plausibility in the context of our dataset.

The threshold behavior of uranium precipitation could offer a potential explanation to the west-east differences in our dataset. Because uranium exists in a soluble state in oxic seawater and becomes immobilized in suboxic and anoxic conditions (Thomson et al., 1990), a threshold behavior is to be expected (Fig. 2). A schematic is provided that illustrates a scenario in which uranium precipitates earlier and much more intensely in the initially less-oxygenated water mass in the Eastern Atlantic (Fig. 9).

At present, the bottom water in the northeast Atlantic is less oxygenated than waters at the same depth in the northwest Atlantic (Fig. 2B). This is because the newly formed, well-oxygenated NADW preferentially spreads southward in the western basin, where it also contributes to a relatively narrow, intense western boundary current (McCartney, 1992; Stommel et al., 1958).

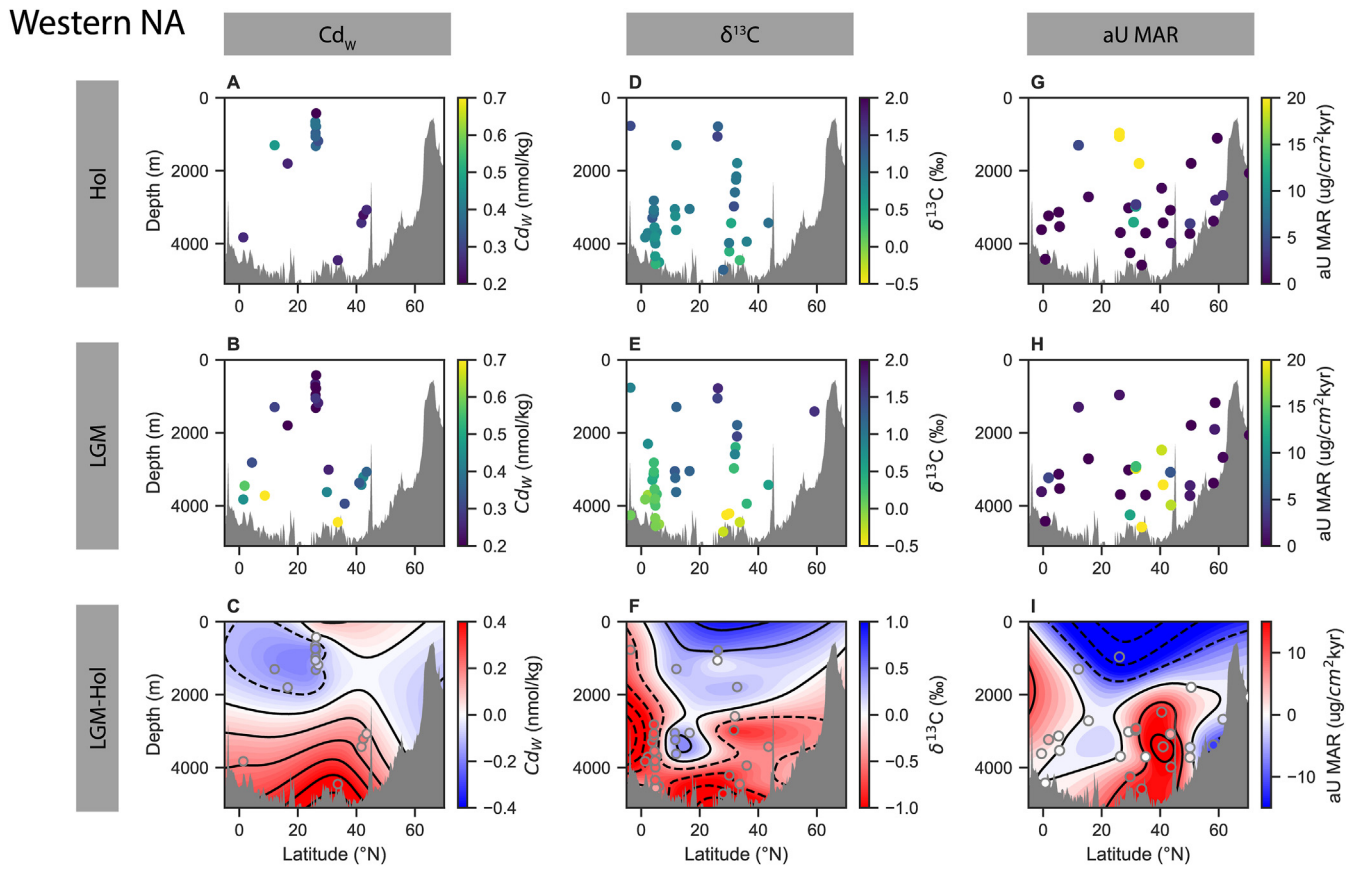

Fig. 7. Comparison of Cd_W (**A, B, C**) (Marchitto and Broecker, 2006), $\delta^{13}C$ (**D, E, F**) (Hesse et al., 2011), and aU MAR (**G, H, I**) datasets in the western North Atlantic transect during the Holocene (**A, D, G**), the LGM (**B, E, H**), and the difference between the two periods (LGM-Holocene; **C, F, I**).

During the LGM, if oxygen level decreased by the same amount across the ocean bottom, the northeast Atlantic bottom water would have reached below the threshold oxygen level for uranium precipitation before those in the northwest Atlantic. The result of our dataset is consistent with this hypothesis (Fig. 4). To verify this hypothesis, future research should better characterize the threshold behavior of aU, potentially by studying modern coretop aU in various settings and making comparisons to the site-adjacent bottom-water and pore-water oxygen levels. We note that the threshold behavior of aU can only potentially explain the west-east differences in our dataset, but not the higher-than-Holocene aU MAR during the LGM that is evident throughout much of the deep North Atlantic. To explain the observed basin-wide decrease in subsurface oxygenation, mechanisms involving changes in export production or ocean circulation must be invoked.

Variations in the flux of organic materials can influence dissolved oxygen concentrations at and beneath the seafloor through the associated changes in respiration. Numerous North Atlantic studies show that glacial productivity was higher than the Holocene, both in the east (Meckler et al., 2013; Romero et al., 2008; Thomson et al., 2000) and the west (Keigwin and Boyle, 2008; Wagner, 2000). These results suggest an enhanced export production that could at least partially explain the increased aU MAR during the LGM compared to the Holocene in large areas of the North Atlantic (Fig. 3). Compilations covering both east and west show no difference in changes between the two basins (Bradtmiller et al., 2007; Heinze and Dittert, 2005), but the coverage is poor for coastal regions where export production was likely higher. Two studies (Menviel et al., 2008; Mix, 1989) suggest higher tropical LGM productivity in the west and lower tropical LGM productivity in the east. The trend reverses in higher latitudes. However, the foraminifera assemblage study (Mix, 1989) results were disputed by a reconstruction based on diatom accumulation rates, which found that the LGM export production in the eastern equatorial Atlantic uniformly increased by an order of magnitude (Abrantes, 2000). In any case, the changes in the tropical Atlantic region of the aU MAR dataset are of the wrong sense (west: low, east: high) to be explained by the productivity pattern seen in the foraminifera assemblage study. At high latitudes, the higher export productivity in the east (Menviel et al., 2008; Mix, 1989) could be consistent with the result of our dataset. Taking the inconclusive evidence as a whole, it appears unlikely that the increased export production in the eastern basin could entirely explain the west-east difference in aU MAR (Fig. 4C, F). Of course, the effect of export productivity, especially in the high latitudes, could simply have enhanced the effects of other factors with stronger influence such as the threshold behavior of aU or the circulation influence discussed below. Future studies to reconstruct the global flux of biogenic opal, $CaCO_3$, total organic carbon, or Ba_{xs}, for the LGM, such as was recently done for the modern ocean (Hayes et al., 2021), may offer more insights. Our analysis shows that the increases in aU concentration and aU MAR cannot solely be explained by the increases in the total carbon export out of euphotic zone (Fig. 10). Nevertheless, we recognize that it is important not to overgeneralize the results of individual aU data points. At a local level, the supply of particulate organic carbon may vary within a basin from site to site. Our aU MAR dataset allows the identification of broad patterns that are unlikely to be solely the result of changes in the local particulate organic carbon supply.

Next, we consider whether our results reflect the differing

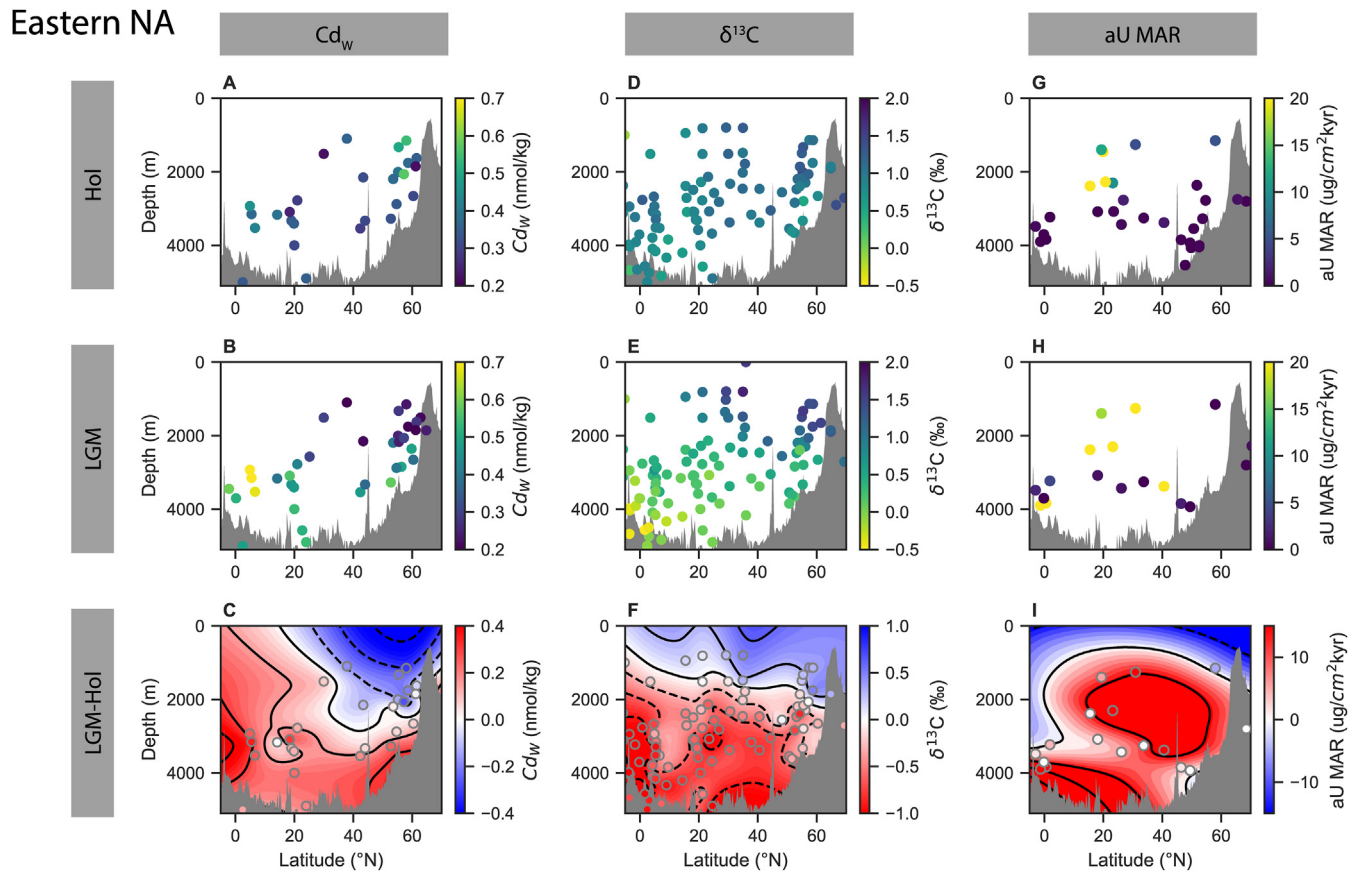

Fig. 8. Comparison of Cd_W (**A, B, C**) (Marchitto and Broecker, 2006), $\delta^{13}C$ (**D, E, F**) (Hesse et al., 2011), and aU MAR (**G, H, I**) datasets in the eastern North Atlantic transect during the Holocene (**A, D, G**), the LGM (**B, E, H**), and the difference between the two periods (LGM-Holocene; **C, F, I**).

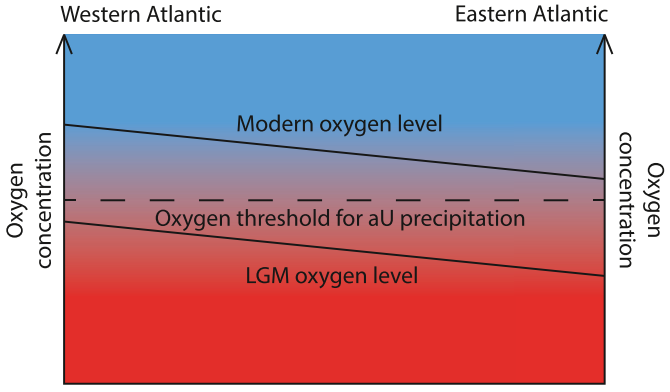

Fig. 9. A schematic illustrating the threshold behavior as a possible explanation of the west-east difference in aU MAR.

water-mass residence times or geometry in the two deep basins. Two water masses from different hemispheres contribute to the deep water in the modern North Atlantic. NADW has its origin in marginal seas of the high latitude North Atlantic and spreads southward circa 2500 m depth. Since it is a newly formed and ventilated deep water mass, today it is rich in oxygen (>260 μmol/kg) (Garcia et al., 2018). AABW originates in the southern hemisphere around Antarctica and spreads northward through the Atlantic basin at >4000 m depth. In contrast to NADW, it is relatively depleted in oxygen (<230 μmol/kg) (Garcia et al., 2018). Our aU MAR dataset could thus suggest that a slowdown in NADW formation led to a substantial increase in the residence time of the deep water, particularly in the eastern basin. An equally consistent explanation is a contrasting glacial water mass geometry within the two basins, with a greater incursion of AABW in the east.

The dynamical evidence for the glacial NADW residence time change is mixed. Studies comparing radiocarbon-based ventilation ages concluded that the deep western North Atlantic was better ventilated than the east during the LGM (Freeman et al., 2016; Skinner et al., 2020). This is consistent with a lower oxygen level in the eastern North Atlantic than the western North Atlantic suggested by our MAR aU dataset. On the other hand, two studies, one of them a compilation of Pa/Th records and the other a modeling study, suggest that the glacial flow rate of northern-sourced waters was higher in the eastern North Atlantic than in the west above 4000 m while the opposite trend is true below 4000 m (Menviel et al., 2020; Ng et al., 2018). The Pa/Th data and radiocarbon-based ventilation age data thus offer conflicting evidence regarding the circulation rate of the waters above 4000 m in the North Atlantic. Although our dataset indicates a more widespread reduction in oxygenation above 4000 m in the east, the magnitude of that reduction is greater in the 35–45°N, 3000–4000 m water depth region in the west (Fig. 4C, F). Therefore, if a water mass in the west experienced acute increase in residence time, but that water mass occupied a limited mid-latitude space, our results could be supportive of that scenario and be consistent with the Pa/Th data. Subsequent studies may seek to explore the feasibility of such a circulation regime. Overall, it is conceivable that changes in the glacial NADW residence time could have primarily influenced the west-east pattern in our dataset, especially considering that other

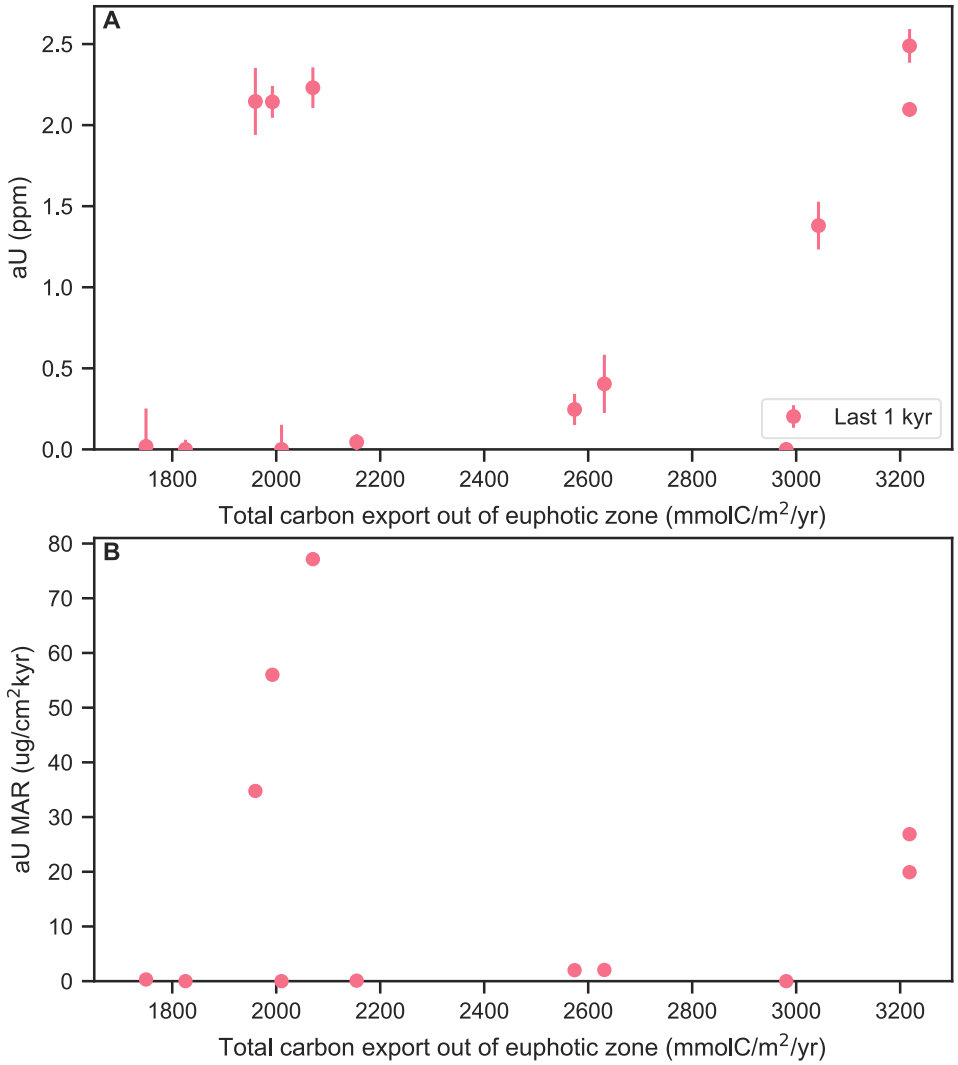

Fig. 10. Scatter plot illustrating the relation between last-millennium aU concentration (A) and aU MAR (B) from our dataset and the total carbon export out of euphotic zone (Nowicki et al., 2022).

factors such as export productivity or the threshold behavior of aU could have modulated that influence.

Regarding the water mass geometry scenario, if a shallower NADW-AABW interface in the eastern basin was the cause of the lower oxygen there, the relatively intense NADW at the western boundary may have countered the incursion of AABW in the western basin (Stommel et al., 1958) and led to an increased AABW presence in the eastern basin. An increased presence of AABW in the eastern basin would have contributed in turn to a shoaling of the water-mass mixing zone there compared to the western basin. As we have shown, the existing $\delta^{13}C$ and Cd_W data are consistent with such changes in the water mass distribution. The inferred continuous glacial presence of NADW in the western basin is also in line with a recent study that presented LGM neodymium isotope records in the region (Pöppelmeier et al., 2020), while the scenario of an intensified AABW presence in the east would be consistent with previous reconstructions of the water masses in the North Atlantic (Curry and Lohmann, 1983; Marchitto and Broecker, 2006; Rickaby et al., 2000).

In summary, the combined evidence for lower dissolved oxygen levels and correspondingly greater carbon storage in the glacial deep North Atlantic, especially within the eastern basin, along with little change or even higher dissolved oxygen concentrations at intermediate depths, are most easily explained by changes in deep ocean circulation that include water mass redistributions. Spatially varying export production or the threshold behavior of aU may also have contributed to the observed changes in dissolved oxygen. We therefore favor the interpretation that changes in deep ocean circulation were primarily responsible for diminished oxygen levels and greater carbon storage in the glacial North Atlantic, and particularly in its deep eastern basin.

5. Conclusions

The aU MAR dataset that we compiled shows that the deep North Atlantic was characterized by substantially lower oxygen concentrations and correspondingly greater carbon storage during the LGM than in the Holocene. A contrast in glacial oxygen levels existed between the east and the west basins. Lower oxygen levels occurred only in the deepest locations in the western basin while similarly low oxygen levels were present throughout the northeast Atlantic. We hypothesize that either the glacial residence time of NADW was longer in the eastern transect, or that a sufficient volume of AABW infilled to occupy a greater depth range. Previous

compilations of two water mass tracers, $\delta^{13}C$ and Cd_W, are consistent with the latter, deep-circulation, interpretations of our aU MAR dataset. The observed threshold behavior of aU or changes in the pattern of export productivity, especially at high latitudes, may also have been contributing factors that enhanced the west-east difference in oxygenation of the glacial North Atlantic that was primarily driven by changes in deep ocean circulation.

Declaration of competing interest

The authors declare that they have no known competing financial interests or personal relationships that could have appeared to influence the work reported in this paper.

Data availability

We have shared the link to the data in Acknowledgements and uploaded the data files.

Acknowledgments

This research used samples and/or data provided by the International Ocean Discovery Program (IODP). We thank the crew of the RRS Discovery, chief scientist Kate Hendry, Laura Robinson, and members of the ICY-LAB team for acquiring GVY005 within ERC grant agreement 678371. This study benefited from discussions with Delia Oppo. We thank Martin Fleisher and Shouyi Wang for assistance in the laboratory. This research was funded by NSF grant AGS 16-35019 to J.F.M and by the IODP Schlanger Fellowship to Y.Z. Y.Z. and J.F.M. jointly initiated the research project, and both contributed to the interpretation of the results and writing of the manuscript. The authors declare no competing interests. The data reported in this paper are archived in Figshare (private link: https://figshare.com/s/2223e286a5797e471e50).

Appendix A. Supplementary data

Supplementary data to this article can be found online at https://doi.org/10.1016/j.quascirev.2022.107914.

References

Abrantes, F., 2000. 200 000 yr diatom records from Atlantic upwelling sites reveal maximum productivity during LGM and a shift in phytoplankton community structure at 185 000 yr. Earth Planet Sci. Lett. 176, 7–16. https://doi.org/10.1016/S0012-821X(99)00312-X.

Adkins, J., deMenocal, P., Eshel, G., 2006. The "African humid period" and the record of marine upwelling from excess230Th in Ocean Drilling Program Hole 658C. Paleoceanography 21, 1–14. https://doi.org/10.1029/2005PA001200.

Algeo, T.J., Li, C., 2020. Redox classification and calibration of redox thresholds in sedimentary systems. Geochimica et Cosmochimica Acta, New developments in geochemical proxies for paleoceanographic research 287, 8–26. https://doi.org/10.1016/j.gca.2020.01.055.

Algeo, T.J., Liu, J., 2020. A re-assessment of elemental proxies for paleoredox analysis. Chem. Geol. 540, 119549. https://doi.org/10.1016/j.chemgeo.2020.119549.

Anderson, R.F., 1982. Concentration, vertical flux, and remineralization of particulate uranium in seawater. Geochem. Cosmochim. Acta 46, 1293–1299. https://doi.org/10.1016/0016-7037(82)90013-8.

Anderson, R.F., Sachs, J.P., Fleisher, M.Q., Allen, K.A., Yu, J., Koutavas, A., Jaccard, S.L., 2019. Deep-Sea oxygen depletion and ocean carbon sequestration during the last ice age. Global Biogeochem. Cycles 33, 301–317. https://doi.org/10.1029/2018GB006049.

Arnold, G.L., Anbar, A.D., Barling, J., Lyons, T.W., 2004. Molybdenum isotope evidence for widespread anoxia in mid-proterozoic oceans. Science 304, 87–90. https://doi.org/10.1126/science.1091785.

Baas, J.H., 1998. Mid-depth oxygen drawdown during Heinrich events: evidence from benthic foraminiferal community structure, trace-fossil tiering, and benthic Ž13C at the Portuguese Margin. Mar. Geol. 31.

Bard, E., Hamelin, B., Fairbanks, R.G., Zindler, A., 1990. Calibration of the ^{14}C timescale over the past 30,000 years using mass spectrometric U–Th ages from Barbados corals. Nature 345, 405–410. https://doi.org/10.1038/345405a0.

Barker, S., Elderfield, H., 2002. Foraminiferal calcification response to glacial-interglacial changes in atmospheric CO 2. Science 297, 833–836. https://doi.org/10.1126/science.1072815.

Barnes, C.E., Cochran, J.K., 1990. Uranium removal in oceanic sediments and the oceanic U balance. Earth Planet Sci. Lett. 97, 94–101. https://doi.org/10.1016/0012-821X(90)90101-3.

Bennett, W.W., Canfield, D.E., 2020. Redox-sensitive trace metals as paleoredox proxies: a review and analysis of data from modern sediments. Earth Sci. Rev. 204, 103175. https://doi.org/10.1016/j.earscirev.2020.103175.

Bond, G.C., Lotti, R., 1995. Iceberg discharges into the North Atlantic on millennial time scales during the last glaciation. Science 267, 1005–1010. https://doi.org/10.1126/science.267.5200.1005.

Boyle, E.A., 1988. The role of vertical chemical fractionation in controlling late Quaternary atmospheric carbon dioxide. J. Geophys. Res.: Oceans 93, 15701–15714. https://doi.org/10.1029/JC093iC12p15701.

Bradtmiller, L.I., Anderson, R.F., Fleisher, M.Q., Burckle, L.H., 2007. Opal burial in the equatorial Atlantic Ocean over the last 30 ka: implications for glacial-interglacial changes in the ocean silicon cycle. Paleoceanography 22, PA4216. https://doi.org/10.1029/2007PA001443.

Bradtmiller, L.I., Anderson, R.F., Sachs, J.P., Fleisher, M.Q., 2010. A deeper respired carbon pool in the glacial equatorial Pacific Ocean. Earth Planet Sci. Lett. 299, 417–425. https://doi.org/10.1016/j.epsl.2010.09.022.

Broecker, W.S., Clark, E., 2001. Glacial-to-Holocene redistribution of carbonate ion in the deep sea. Science 294, 2152–2155. https://doi.org/10.1126/science.1064171.

Broecker, W.S., Maier-Reimer, E., 1992. The influence of air and sea exchange on the carbon isotope distribution in the sea. Global Biogeochem. Cycles 6, 315–320. https://doi.org/10.1029/92GB01672.

Chase, Z., Anderson, R.F., Fleisher, M.Q., 2001. Evidence from authigenic uranium for increased productivity of the glacial subantarctic ocean. Paleoceanography 16, 468–478. https://doi.org/10.1029/2000PA000542.

Cheng, H., Lawrence Edwards, R., Shen, C.-C., Polyak, V.J., Asmerom, Y., Woodhead, J., Hellstrom, J., Wang, Y., Kong, X., Spötl, C., Wang, X., Calvin Alexander, E., 2013. Improvements in ^{230}Th dating, ^{230}Th and ^{234}U half-life values, and U–Th isotopic measurements by multi-collector inductively coupled plasma mass spectrometry. Earth Planet Sci. Lett. 371 (372), 82–91. https://doi.org/10.1016/j.epsl.2013.04.006.

Cochran, J.K., Carey, A.E., Sholkovitz, E.R., Surprenant, L.D., 1986. The geochemistry of uranium and thorium in coastal marine sediments and sediment pore waters. Geochem. Cosmochim. Acta 50, 663–680. https://doi.org/10.1016/0016-7037(86)90344-3.

Colley, S., Thomson, J., 1985. Recurrent uranium relocations in distal turbidites emplaced in pelagic conditions. Geochem. Cosmochim. Acta 49, 2339–2348. https://doi.org/10.1016/0016-7037(85)90234-0.

Colley, S., Thomson, J., Toole, J., 1989. Uranium relocations and derivation of quasi-isochrons for a turbidite/pelagic sequence in the Northeast Atlantic. Geochem. Cosmochim. Acta 53, 1223–1234. https://doi.org/10.1016/0016-7037(89)90058-6.

Costa, K.M., Hayes, C.T., Anderson, R.F., Pavia, F.J., Bausch, A., Deng, F., Dutay, J., Geibert, W., Heinze, C., Henderson, G., Hillaire-Marcel, C., Hoffmann, S., Jaccard, S.L., Jacobel, A.W., Kienast, S.S., Kipp, L., Lerner, P., Lippold, J., Lund, D., Marcantonio, F., McGee, D., McManus, J.F., Mekik, F., Middleton, J.L., Missiaen, L., Not, C., Pichat, S., Robinson, L.F., Rowland, G.H., Roy-Barman, M., Tagliabue, A., Torfstein, A., Winckler, G., Zhou, Y., 2020. ^{230}Th normalization: new insights on an essential tool for quantifying sedimentary fluxes in the modern and quaternary ocean. Paleoceanogr. Paleoclimatol. 35. https://doi.org/10.1029/2019PA003820.

Curry, W.B., Lohmann, G.P., 1983. Reduced advection into Atlantic Ocean deep eastern basins during last glaciation maximum. Nature 306, 577–580. https://doi.org/10.1038/306577a0.

Curry, W.B., Oppo, D.W., 2005. Glacial water mass geometry and the distribution of $\delta^{13}C$ of CO_2 in the western Atlantic Ocean. Paleoceanography 20, 1–12. https://doi.org/10.1029/2004PA001021.

Dean, W.E., 2007. Sediment geochemical records of productivity and oxygen depletion along the margin of western North America during the past 60,000 years: teleconnections with Greenland Ice and the Cariaco Basin. Quaternary Science Reviews 26, 98–114. https://doi.org/10.1016/j.quascirev.2006.08.006.

Diaz, R., Rosenberg, R., 1995. Marine benthic hypoxia: a review of its ecological effects and the behavioural responses of benthic macrofauna. Oceanogr. Mar. Biol. Annu. Rev. 33 (Oceanography and Marine Biology).

Diaz, R.J., Rosenberg, R., 2008. Spreading dead zones and consequences for marine ecosystems. Science 321, 926–929. https://doi.org/10.1126/science.1156401.

Dunk, R.M., Mills, R.A., Jenkins, W.J., 2002. A reevaluation of the oceanic uranium budget for the Holocene. Chem. Geol., Geochem. Crust. Fluid.-Fluid Crust Chem. Fluxes Earth's Surface 190, 45–67. https://doi.org/10.1016/S0009-2541(02)00110-9.

Fleisher, M.Q., Anderson, R.F., 1991. Particulate matter digestion and radionuclide blanks. Geophys. Monogr. 63, 221–222.

Foster, G.L., Rae, J.W.B., 2016. Reconstructing Ocean pH with boron isotopes in foraminifera. Annu. Rev. Earth Planet Sci. 44, 207–237. https://doi.org/10.1146/annurev-earth-060115-012226.

Francis, A.J., Dodge, C.J., Lu, Fulong, Halada, G.P., Clayton, C.R., 1994. XPS and XANES studies of uranium reduction by Clostridium sp. Environ. Sci. Technol. 28, 636–639. https://doi.org/10.1021/es00053a016.

Francois, R., Bacon, M.P., Altabet, M.A., Labeyrie, L.D., 1993. Glacial/interglacial changes in sediment rain rate in the SW Indian Sector of subantarctic Waters as recorded by ^{230}Th, ^{231}Pa, U, and $\delta^{15}N$. Paleoceanography 8, 611–629. https://

doi.org/10.1029/93PA00784.
Frank, M., Eisenhauer, A., 1996. Radionuclides Analysed on Sediment Core PS1533-3 from the Arctic Ocean. https://doi.org/10.1594/PANGAEA.50830.
Freeman, E., Skinner, L.C., Waelbroeck, C., Hodell, D., 2016. Radiocarbon evidence for enhanced respired carbon storage in the Atlantic at the Last Glacial Maximum. Nat. Commun. 7, 11998. https://doi.org/10.1038/ncomms11998.
Garcia, H.E., Weathers, K., Paver, C.R., Smolyar, I., Boyer, T.P., Locarnini, R.A., Zweng, M.M., Mishonov, A.V., Baranova, O.K., Seidov, D., Reagan, J.R., 2018. World Ocean Atlas 2018, volume 3: dissolved oxygen, apparent oxygen utilization, and oxygen saturation. NOAA Atlas NESDIS 83, 33.
Gebbie, G., 2014. How much did glacial North Atlantic water shoal? Paleoceanography 29, 190–209. https://doi.org/10.1002/2013PA002557.
Gottschalk, J., Skinner, L.C., Lippold, J., Vogel, H., Frank, N., Jaccard, S.L., Waelbroeck, C., 2016. Biological and physical controls in the Southern Ocean on past millennial-scale atmospheric CO2changes. Nat. Commun. 7. https://doi.org/10.1038/ncomms11539.
Haug, G.H., Pedersen, T.F., Sigman, D.M., Calvert, S.E., Nielsen, B., Peterson, L.C., 1998. Glacial/interglacial variations in production and nitrogen fixation in the Cariaco Basin during the last 580 kyr. Paleoceanography 13, 427–432. https://doi.org/10.1029/98PA01976.
Hayes, C.T., Costa, K.M., Anderson, R.F., Calvo, E., Chase, Z., Demina, L.L., Dutay, J., German, C.R., Heimbürger-Boavida, L., Jaccard, S.L., Jacobel, A., Kohfeld, K.E., Kravchishina, M.D., Lippold, J., Mekik, F., Missiaen, L., Pavia, F.J., Paytan, A., Pedrosa-Pamies, R., Petrova, M.V., Rahman, S., Robinson, L.F., Roy-Barman, M., Sanchez-Vidal, A., Shiller, A., Tagliabue, A., Tessin, A.C., van Hulten, M., Zhang, J., 2021. Global Ocean sediment composition and burial flux in the deep sea. Global Biogeochem. Cycles 35. https://doi.org/10.1029/2020GB006769.
Heinze, C., Dittert, N., 2005. Impact of paleocirculations on the silicon redistribution in the world ocean. Mar. Geol. 214, 201–213. https://doi.org/10.1016/j.margeo.2004.10.026.
Henderson, G.M., Anderson, R.F., 2003. The U-series toolbox for paleoceanography. Rev. Mineral. Geochem. 52, 493–531. https://doi.org/10.2113/0520493.
Hendry, K.R., Huvenne, V.A.I., Robinson, L.F., Annett, A., Badger, M., Jacobel, A.W., Ng, H.C., Opher, J., Pickering, R.A., Taylor, M.L., Bates, S.L., Cooper, A., Cushman, G.G., Goodwin, C., Hoy, S., Rowland, G., Samperiz, A., Williams, J.A., Achterberg, E.P., Arrowsmith, C., Alexander Brearley, J., Henley, S.F., Krause, J.W., Leng, M.J., Li, T., McManus, J.F., Meredith, M.P., Perkins, R., Woodward, E.M.S., 2019. The biogeochemical impact of glacial meltwater from Southwest Greenland. Prog. Oceanogr. 176, 102126. https://doi.org/10.1016/j.pocean.2019.102126.
Hesse, T., Butzin, M., Bickert, T., Lohmann, G., 2011. A model-data comparison of $\delta^{13}C$ in the glacial Atlantic Ocean. Paleoceanography 26. https://doi.org/10.1029/2010PA002085.
Hoogakker, B.A.A., Elderfield, H., Schmiedl, G., McCave, I.N., Rickaby, R.E.M., 2015. Glacial-interglacial changes in bottom-water oxygen content on the Portuguese margin. Nat. Geosci. 8, 40–43. https://doi.org/10.1038/ngeo2317.
Jaccard, S.L., Galbraith, E.D., 2012. Large climate-driven changes of oceanic oxygen concentrations during the last deglaciation. Nat. Geosci. 5, 151–156. https://doi.org/10.1038/ngeo1352.
Jaccard, S.L., Galbraith, E.D., Martínez-Garciá, A., Anderson, R.F., 2016. Covariation of deep Southern Ocean oxygenation and atmospheric CO_2 through the last ice age. Nature 530, 207–210. https://doi.org/10.1038/nature16514.
Jacobel, A.W., Anderson, R.F., Jaccard, S.L., McManus, J.F., Pavia, F.J., Winckler, G., 2020. Deep Pacific storage of respired carbon during the last ice age: perspectives from bottom water oxygen reconstructions. Quat. Sci. Rev. 230, 106065. https://doi.org/10.1016/j.quascirev.2019.106065.
Janssen, D.J., Conway, T.M., John, S.G., Christian, J.R., Kramer, D.I., Pedersen, T.F., Cullen, J.T., 2014. Undocumented water column sink for cadmium in open ocean oxygen-deficient zones. Proc. Natl. Acad. Sci. USA 111, 6888–6893. https://doi.org/10.1073/pnas.1402388111.
Keigwin, L.D., Boyle, E.A., 2008. Did North Atlantic overturning halt 17,000 years ago? Paleoceanography 23, PA1101. https://doi.org/10.1029/2007PA001500.
Klinkhammer, G.P., Palmer, M.R., 1991. Uranium in the oceans: where it goes and why. Geochem. Cosmochim. Acta 55, 1799–1806. https://doi.org/10.1016/0016-7037(91)90024-Y.
Ku, T.-L., Knauss, K.G., Mathieu, G.G., 1977. Uranium in open ocean: concentration and isotopic composition. Deep-Sea Res. 24, 1005–1017. https://doi.org/10.1016/0146-6291(77)90571-9.
Kumar, N., Anderson, R.F., Mortlock, R.A., Froelich, P.N., Kubik, P., Dittrich-Hannen, B., Suter, M., 1995. Increased biological productivity and export production in the glacial Southern Ocean. Nature 378, 675. https://doi.org/10.1038/378675a0.
Langmuir, D., 1978. Uranium solution-mineral equilibria at low temperatures with applications to sedimentary ore deposits. Geochem. Cosmochim. Acta 42, 547–569. https://doi.org/10.1016/0016-7037(78)90001-7.
Li, W.-X., Lundberg, J., Dickin, A.P., Ford, D.C., Schwarcz, H.P., McNutt, R., Williams, D., 1989. High-precision mass-spectrometric uranium-series dating of cave deposits and implications for palaeoclimate studies. Nature 339, 534–536. https://doi.org/10.1038/339534a0.
Lippold, J., Gutjahr, M., Blaser, P., Christner, E., de Carvalho Ferreira, M.L., Mulitza, S., Christl, M., Wombacher, F., Böhm, E., Antz, B., Cartapanis, O., Vogel, H., Jaccard, S.L., 2016. Deep water provenance and dynamics of the (de)glacial Atlantic meridional overturning circulation. Earth Planet Sci. Lett. 445, 68–78. https://doi.org/10.1016/j.epsl.2016.04.013.
Lovley, D.R., Phillips, E.J., 1992. Reduction of uranium by Desulfovibrio desulfuricans. Appl. Environ. Microbiol. 58, 850–856. https://doi.org/10.1128/aem.58.3.850-856.1992.
Lovley, D.R., Phillips, E.J.P., Gorby, Y.A., Landa, E.R., 1991. Microbial reduction of uranium. Nature 350, 413–416. https://doi.org/10.1038/350413a0.
Lovley, D.R., Roden, E.E., Phillips, E.J.P., Woodward, J.C., 1993. Enzymatic iron and uranium reduction by sulfate-reducing bacteria. Mar. Geol., Marin. Sediments, Burial, Pore Water Chem., Microbiol. Diagenesis 113, 41–53. https://doi.org/10.1016/0025-3227(93)90148-O.
Lu, W., Wang, Y., Oppo, D.W., Nielsen, S.G., Costa, K.M., 2022. Comparing paleoxygenation proxies (benthic foraminiferal surface porosity, I/Ca, authigenic uranium) on modern sediments and the glacial Arabian Sea. Geochem. Cosmochim. Acta 331, 69–85. https://doi.org/10.1016/j.gca.2022.06.001.
Lynch-Stieglitz, J., 2003. 6.16 - tracers of past ocean circulation. In: Holland, H.D., Turekian, K.K. (Eds.), Treatise on Geochemistry. Pergamon, Oxford, pp. 433–451. https://doi.org/10.1016/B0-08-043751-6/06117-X.
Lynch-Stieglitz, J., Stocker, T.F., Broecker, W.S., Fairbanks, R.G., 1995. The influence of air-sea exchange on the isotopic composition of oceanic carbon: observations and modeling. Global Biogeochem. Cycles 9, 653–665. https://doi.org/10.1029/95GB02574.
Mangini, A., 1978. Thorium and uranium isotope analyses on" Meteor" core 12310, NW African continental rise. Meteor Forschungsergeb 29, 1–5.
Mangini, A., Jung, M., Laukenmann, S., 2001. What do we learn from peaks of uranium and of manganese in deep sea sediments? Mar. Geol. 177, 63–78. https://doi.org/10.1016/S0025-3227(01)00124-4.
Marchitto, T.M., Broecker, W.S., 2006. Deep water mass geometry in the glacial Atlantic Ocean: a review of constraints from the paleonutrient proxy Cd/Ca. G-cubed 7. https://doi.org/10.1029/2006GC001323.
Martinez, P., Bertrand, P., Calvert, S.E., Pedersen, T.F., Shimmield, G.B., Lallier-Vergès, E., Fontugne, M.R., 2000. Spatial variations in nutrient utilization, production and diagenesis in the sediments of a coastal upwelling regime (NW Africa): Implications for the paleoceanographic record. Journal of Marine Research 58, 809–835. https://doi.org/10.1357/002224000321358927.
McCartney, M., 1992. Recirculating components to the deep boundary current of the northern North Atlantic. Prog. Oceanogr. 29, 283–383.
McCorkle, D.C., Emerson, S.R., 1988. The relationship between pore water carbon isotopic composition and bottom water oxygen concentration. Geochem. Cosmochim. Acta 52, 1169–1178. https://doi.org/10.1016/0016-7037(88)90270-0.
McCorkle, D.C., Keigwin, L.D., Corliss, B.H., Emerson, S.R., 1990. The influence of microhabitats on the carbon isotopic composition of deep-sea benthic foraminifera. Paleoceanography 5, 161–185. https://doi.org/10.1029/PA005i002p00161.
McManus, J., Berelson, W.M., Klinkhammer, G.P., Hammond, D.E., Holm, C., 2005. Authigenic uranium: relationship to oxygen penetration depth and organic carbon rain. Geochem. Cosmochim. Acta 69, 95–108. https://doi.org/10.1016/j.gca.2004.06.023.
McManus, J.F., Anderson, R.F., Broecker, W.S., Fleisher, M.Q., Higgins, S.M., 1998. Radiometrically determined sedimentary fluxes in the sub-polar North Atlantic during the last 140,000 years. Earth Planet Sci. Lett. 155, 29–43. https://doi.org/10.1016/S0012-821X(97)00201-X.
McManus, J.F., Francois, R., Gherardl, J.M., Kelgwin, L., Drown-Leger, S., 2004. Collapse and rapid resumption of Atlantic meridional circulation linked to deglacial climate changes. Nature 428, 834–837. https://doi.org/10.1038/nature02494.
Meckler, A.N., Sigman, D.M., Gibson, K.A., François, R., Martínez-García, A., Jaccard, S.L., Röhl, U., Peterson, L.C., Tiedemann, R., Haug, G.H., 2013. Deglacial pulses of deep-ocean silicate into the subtropical North Atlantic Ocean. Nature 495, 495–498. https://doi.org/10.1038/nature12006.
Menviel, L., Timmermann, A., Mouchet, A., Timm, O., 2008. Meridional reorganizations of marine and terrestrial productivity during Heinrich events: dynamic CO_2 response to a freshwater input. Paleoceanography 23. https://doi.org/10.1029/2007PA001445.
Menviel, L., Yu, J., Joos, F., Mouchet, A., Meissner, K.J., England, M.H., 2017. Poorly ventilated deep ocean at the Last Glacial Maximum inferred from carbon isotopes: a data-model comparison study: LGM $\delta^{13}C$. Paleoceanography 32, 2–17. https://doi.org/10.1002/2016PA003024.
Menviel, L.C., Spence, P., Skinner, L.C., Tachikawa, K., Friedrich, T., Missiaen, L., Yu, J., 2020. Enhanced mid-depth southward transport in the northeast Atlantic at the last glacial maximum despite a weaker AMOC. Paleoceanogr. Paleoclimatol. 35. https://doi.org/10.1029/2019PA003793.
Missiaen, L., Pichat, S., Waelbroeck, C., Douville, E., Bordier, L., Dapoigny, A., Thil, F., Foliot, L., Wacker, L., 2018. Downcore variations of sedimentary detrital (238U/232Th) ratio: implications on the use of230Thxsand231Paxsto reconstruct sediment flux and ocean circulation. G-cubed 19, 2560–2573. https://doi.org/10.1029/2017GC007410.
Mix, A.C., 1989. Influence of productivity variations on long-term atmospheric CO_2. Nature 337, 541–544. https://doi.org/10.1038/337541a0.
Mix, A.C., Bard, E., Schneider, R., 2001. Environmental processes of the ice age: land, oceans, glaciers (EPILOG). Quat. Sci. Rev. 20, 627–657. https://doi.org/10.1016/S0277-3791(00)00145-1.
Morford, J.L., Emerson, S., 1999. The geochemistry of redox sensitive trace metals in sediments. Geochem. Cosmochim. Acta 63, 1735–1750. https://doi.org/10.1016/S0016-7037(99)00126-X.
Naafs, B.D.A., Hefter, J., Grützner, J., Stein, R., 2013. Warming of surface waters in the mid-latitude North Atlantic during Heinrich events. Paleoceanography 28, 153–163. https://doi.org/10.1029/2012PA002354.

Ng, H.C., Robinson, L.F., McManus, J.F., Mohamed, K.J., Jacobel, A.W., Ivanovic, R.F., Gregoire, L.J., Chen, T., 2018. Coherent deglacial changes in western Atlantic Ocean circulation. Nat. Commun. 9, 2947. https://doi.org/10.1038/s41467-018-05312-3.

Nowicki, M., DeVries, T., Siegel, D.A., 2022. Quantifying the carbon export and sequestration pathways of the Ocean's biological carbon pump. Global Biogeochem. Cycles 36, e2021GB007083. https://doi.org/10.1029/2021GB007083.

Oppo, D.W., Fairbanks, R.G., 1989. Carbon isotope composition of tropical surface water during the past 22,000 years. Paleoceanography 4, 333–351. https://doi.org/10.1029/PA004i004p00333.

Oppo, D.W., Gebbie, G., Huang, K., Curry, W.B., Marchitto, T.M., Pietro, K.R., 2018. Data constraints on glacial atlantic water mass geometry and properties. Paleoceanogr. Paleoclimatol. 33, 1013–1034. https://doi.org/10.1029/2018PA003408.

Oppo, D.W., Horowitz, M., 2000. Glacial deep water geometry: south Atlantic benthic foraminiferal Cd/Ca and δ13C evidence. Paleoceanography 15, 147–160. https://doi.org/10.1029/1999PA000436.

Pöppelmeier, F., Blaser, P., Gutjahr, M., Jaccard, S.L., Frank, M., Max, L., Lippold, J., 2020. Northern-sourced water dominated the atlantic ocean during the last glacial maximum. Geology 48, 826–829. https://doi.org/10.1130/G47628.1.

Rae, J.W.B., Foster, G.L., Schmidt, D.N., Elliott, T., 2011. Boron isotopes and B/Ca in benthic foraminifera: proxies for the deep ocean carbonate system. Earth Planet Sci. Lett. 302, 403–413. https://doi.org/10.1016/j.epsl.2010.12.034.

Reimer, P.J., Bard, E., Bayliss, A., Beck, J.W., Blackwell, P.G., Ramsey, C.B., Buck, C.E., Cheng, H., Edwards, R.L., Friedrich, M., Grootes, P.M., Guilderson, T.P., Haflidason, H., Hajdas, I., Hatté, C., Heaton, T.J., Hoffmann, D.L., Hogg, A.G., Hughen, K.A., Kaiser, K.F., Kromer, B., Manning, S.W., Niu, M., Reimer, R.W., Richards, D.A., Scott, E.M., Southon, J.R., Staff, R.A., Turney, C.S.M., van der Plicht, J., 2013. IntCal13 and Marine13 radiocarbon age calibration curves 0–50,000 Years cal BP. Radiocarbon 55, 1869–1887. https://doi.org/10.2458/azu_js_rc.55.16947.

Rickaby, R.E.M., Greaves, M.J., Elderfield, H., 2000. Cd in planktonic and benthic foraminiferal shells determined by thermal ionisation mass spectrometry. Geochem. Cosmochim. Acta 64, 1229–1236. https://doi.org/10.1016/S0016-7037(99)00317-8.

Riedinger, N., Scholz, F., Abshire, M.L., Zabel, M., 2021. Persistent deep water anoxia in the eastern South Atlantic during the last ice age. Proc. Natl. Acad. Sci. USA 118. https://doi.org/10.1073/pnas.2107034118.

Romero, O.E., Kim, J.-H., Donner, B., 2008. Submillennial-to-millennial variability of diatom production off Mauritania, NW Africa, during the last glacial cycle. Paleoceanography 23, PA3218. https://doi.org/10.1029/2008PA001601.

Sani, R.K., Peyton, B.M., Amonette, J.E., Geesey, G.G., 2004. Reduction of uranium(VI) under sulfate-reducing conditions in the presence of Fe(III)-(hydr)oxides 1 1 Associate editor: C. M. Eggleston. Geochem. Cosmochim. Acta 68, 2639–2648. https://doi.org/10.1016/j.gca.2004.01.005.

Sarnthein, M., Schneider, B., Grootes, P.M., 2013. Peak glacial ^{14}C ventilation ages suggest major draw-down of carbon into the abyssal ocean. Clim. Past 9, 2595–2614. https://doi.org/10.5194/cp-9-2595-2013.

Schmittner, A., Bostock, H.C., Cartapanis, O., Curry, W.B., Filipsson, H.L., Galbraith, E.D., Gottschalk, J., Herguera, J.C., Hoogakker, B., Jaccard, S., Lisiecki, L.E., Lund, D.C., Martínez-Méndez, G., Lynch-Stieglitz, J., Mackensen, A., Michel, E., Mix, A.C., Oppo, D.W., Peterson, C.D., Repschläger, J., Sikes, E.L., Spero, H.J., Waelbroeck, C., 2017. Calibration of the carbon isotope composition ($\delta^{13}C$) of benthic foraminifera. Paleoceanography. https://doi.org/10.1002/2016PA003072, 1–19.

Schönfeld, J., Zahn, R., de Abreu, L., 2003. Surface and deep water response to rapid climate changes at the Western Iberian Margin. Global Planet. Change 36, 237–264. https://doi.org/10.1016/S0921-8181(02)00197-2.

Senko, J.M., Istok, J.D., Suflita, J.M., Krumholz, L.R., 2002. In-situ evidence for uranium immobilization and remobilization. Environ. Sci. Technol. 36, 1491–1496. https://doi.org/10.1021/es011240x.

Shaw, T.J., Sholkovitz, E.R., Klinkhammer, G., 1994. Redox dynamics in the Chesapeake Bay: the effect on sediment/water uranium exchange. Geochem. Cosmochim. Acta 58, 2985–2995. https://doi.org/10.1016/0016-7037(94)90173-2.

Siebert, C., Nägler, T.F., von Blanckenburg, F., Kramers, J.D., 2003. Molybdenum isotope records as a potential new proxy for paleoceanography. Earth Planet Sci. Lett. 211, 159–171. https://doi.org/10.1016/S0012-821X(03)00189-4.

Skinner, L.C., Freeman, E., Hodell, D., Waelbroeck, C., Riveiros, N.V., Scrivner, A.E., 2020. Atlantic Ocean ventilation changes across the last deglaciation and their carbon cycle implications. Paleoceanogr. Paleoclimatol. https://doi.org/10.1029/2020PA004074.

Sosdian, S.M., Rosenthal, Y., Toggweiler, J.R., 2018. Deep atlantic carbonate ion and $CaCO_3$ compensation during the ice ages. Paleoceanogr. Paleoclimatol. 33, 546–562. https://doi.org/10.1029/2017PA003312.

Stommel, H., Arons, A.B., Faller, A.J., 1958. Some examples of stationary planetary flow patterns in bounded basins. Tellus 10, 179–187. https://doi.org/10.3402/tellusa.v10i2.9238.

Stramma, L., Prince, E.D., Schmidtko, S., Luo, J., Hoolihan, J.P., Visbeck, M., Wallace, D.W.R., Brandt, P., Körtzinger, A., 2012. Expansion of oxygen minimum zones may reduce available habitat for tropical pelagic fishes. Nat. Clim. Change 2, 33–37. https://doi.org/10.1038/nclimate1304.

Streeter, S.S., Shackleton, N.J., 1979. Paleocirculation of the deep North Atlantic: 150,000-year record of benthic foraminifera and oxygen-18. Sci., New Series 203, 168–171.

Thomas, N.C., Bradbury, H.J., Hodell, D.A., 2022. Changes in North Atlantic deep-water oxygenation across the middle pleistocene transition. Science 377, 654–659. https://doi.org/10.1126/science.abj7761.

Thomson, J., Nixon, S., Summerhayes, C.P., Rohling, E.J., Schönfeld, J., Zahn, R., Grootes, P., Abrantes, F., Gaspar, L., Vaqueiro, S., 2000. Enhanced productivity on the Iberian margin during glacial/interglacial transitions revealed by barium and diatoms. J. Geol. Soc. 157, 667–677. https://doi.org/10.1144/jgs.157.3.667.

Thomson, J., Wallace, H.E., Colley, S., Toole, J., 1990. Authigenic uranium in Atlantic sediments of the last glacial stage - a diagenetic phenomenon. Earth Planet Sci. Lett. 98, 222–232. https://doi.org/10.1016/0012-821X(90)90061-2.

Tucker, M.D., Barton, L.L., Thomson, B.M., 1996. Kinetic coefficients for simultaneous reduction of sulfate and uranium by Desulfovibrio desulfuricans. Appl. Microbiol. Biotechnol. 46, 74–77. https://doi.org/10.1007/s002530050785.

Vaquer-Sunyer, R., Duarte, C.M., 2008. Thresholds of hypoxia for marine biodiversity. Proc. Natl. Acad. Sci. USA 105, 15452–15457. https://doi.org/10.1073/pnas.0803833105.

Volk, T., Hoffert, M.I., 1985. Ocean carbon pumps: analysis of relative strengths and efficiencies in ocean-driven atmospheric CO_2 changes. In: Sundquist, E.T., Broecker, W.S. (Eds.), Geophysical Monograph Series. American Geophysical Union, Washington, D. C., pp. 99–110. https://doi.org/10.1029/GM032p0099

Wagner, T., 2000. Control of organic carbon accumulation in the late quaternary equatorial atlantic (Ocean Drilling Program sites 664 and 663): productivity versus terrigenous supply. Paleoceanography 15, 181–199. https://doi.org/10.1029/1999PA000406.

Yarincik, K.M., Murray, R.W., Lyons, T.W., Peterson, L.C., Haug, G.H., 2000. Oxygenation history of bottom waters in the Cariaco Basin, Venezuela, over the past 578,000 years: results from redox-sensitive metals (Mo, V, Mn, and Fe). Paleoceanography 15, 593–604. https://doi.org/10.1029/1999PA000401.

Yu, J., Broecker, W.S., Elderfield, H., Jin, Z., McManus, J., Zhang, F., 2010. Loss of Carbon from the Deep Sea Since the Last Glacial Maximum. Science 330, 1084–1087. https://doi.org/10.1126/science.1193221.

Yu, J., Menviel, L., Jin, Z.D., Thornalley, D.J.R., Barker, S., Marino, G., Rohling, E.J., Cai, Y., Zhang, F., Wang, X., Dai, Y., Chen, P., Broecker, W.S., 2016. Sequestration of carbon in the deep Atlantic during the last glaciation. Nat. Geosci. 9, 319–324. https://doi.org/10.1038/ngeo2657.

Zheng, Y., Anderson, R.F., van Geen, A., Fleisher, M.Q., 2002. Remobilization of authigenic uranium in marine sediments by bioturbation. Geochem. Cosmochim. Acta 66, 1759–1772. https://doi.org/10.1016/S0016-7037(01)00886-9.

Zhou, Y., McManus, J.F., Jacobel, A.W., Costa, K.M., Wang, S., Alvarez Caraveo, B., 2021. Enhanced iceberg discharge in the western North Atlantic during all Heinrich events of the last glaciation. Earth Planet Sci. Lett. 564, 116910. https://doi.org/10.1016/j.epsl.2021.116910.